

• Article •
SPECIAL TOPIC:

Einstein Probe discovery of EP240408a: a peculiar X-ray transient with an intermediate timescale

Wenda Zhang^{1*}, Weimin Yuan^{1,2*}, Zhixing Ling^{1,2*}, Yong Chen^{3*}, Nanda Rea^{4,5*}, Arne Rau^{6*}, Zhiming Cai⁷, Huaqing Cheng¹, Francesco Coti Zelati^{4,5}, Lixin Dai⁸, Jingwei Hu¹, Shumei Jia³, Chichuan Jin^{1,2}, Dongyue Li¹, Paul O'Brien⁹, Rongfeng Shen¹⁰, Xinwen Shu¹¹, Shengli Sun¹², Xiaojin Sun¹², Xiaofeng Wang¹³, Lei Yang¹¹, Bing Zhang^{14,15}, Chen Zhang¹, Shuang-Nan Zhang^{3,2}, Yonghe Zhang⁷, Jie An^{1,2}, David Buckley^{16,17,18}, Alexis Coleiro¹⁹, Bertrand Cordier²⁰, Liming Dou²¹, Rob Eyles-Ferris⁹, Zhou Fan^{1,2}, Hua Feng³, Shaoyu Fu^{1,2}, Johan P. U. Fynbo^{22,23}, Lluís Galbany^{4,5}, Saurabh W. Jha²⁴, Shuaiqing Jiang^{1,2}, Albert Kong²⁵, Erik Kuulkers²⁶, Weihua Lei²⁷, Wenxiong Li¹, Bifang Liu^{1,2}, Mingjun Liu^{1,2}, Xing Liu^{1,2}, Yuan Liu¹, Zhu Liu⁶, Chandreyee Maitra⁶, Alessio Marino^{4,5}, Itumeleng Monageng^{16,17}, Kirpal Nandra⁶, Jeremy Sanders⁶, Roberto Soria^{2,28,29}, Lian Tao³, Junfeng Wang³⁰, Song Wang^{1,31}, Tinggui Wang^{32,33,34}, Zhongxiang Wang^{35,36}, Qingwen Wu²⁷, Xuefeng Wu^{37,33}, Dong Xu¹, Yanjun Xu³, Suijian Xue¹, Yongquan Xue^{38,32,33}, Zijian Zhang⁸, Zipei Zhu¹, Hu Zou¹, Congying Bao¹, Fansheng Chen¹², Houlei Chen^{39,2}, Tianxiang Chen³, Wei Chen^{1,2}, Yehai Chen⁷, Yifan Chen¹², Chenzhou Cui^{1,2}, Weiwei Cui³, Yanfeng Dai¹, Dongwei Fan¹, Ju Guan³, Dawei Han³, Dongjie Hou³, Haibo Hu¹, Maohai Huang^{1,2}, Jia Huo³, Zhenqing Jia¹, Bowen Jiang⁴⁰, Ge Jin⁴⁰, Chengkui Li³, Junfei Li¹², Longhui Li⁴⁰, Maoshun Li³, Wei Li³, Zhengda Li¹², Tianying Lian^{1,2}, Congzhan Liu³, Heyang Liu¹, Huaqiu Liu⁷, Fangjun Lu³, Laidan Luo³, Jia Ma³, Xuan Mao^{1,2}, Haiwu Pan¹, Xin Pan¹, Liming Song³, Hui Sun¹, Yunyin Tan⁴¹, Qingjun Tang^{39,2}, Yihan Tao¹, Hao Wang³, Juan Wang³, Lei Wang⁴², Wenxin Wang¹, Yilong Wang^{1,2}, Yusa Wang³, Qinyu Wu^{1,2}, Haitao Xu⁴¹, Jingjing Xu³, Xinpeng Xu^{1,2}, Yunfei Xu^{1,2}, Zhao Xu⁴⁰, Changbin Xue⁴¹, Yulong Xue¹², Ailiang Yan¹², Haonan Yang^{1,2}, Xiongtao Yang³, Yanji Yang³, Juan Zhang³, Mo Zhang¹, Wenjie Zhang¹, Zhen Zhang^{1,2}, Zhen Zhang⁴⁰, Ziliang Zhang³, Donghua Zhao¹, Haisheng Zhao³, Xiaofan Zhao³, Zijian Zhao³, Hongyan Zhou^{43,44,34}, Yilin Zhou⁷, Yuxuan Zhu³, and Zhencai Zhu⁷

arXiv:2410.21617v1 [astro-ph.HE] 28 Oct 2024

- ¹National Astronomical Observatories, Chinese Academy of Sciences, Beijing 100101, People's Republic of China;
- ²School of Astronomy and Space Sciences, University of Chinese Academy of Sciences, Beijing 100049, People's Republic of China;
- ³Key Laboratory of Particle Astrophysics, Institute of High Energy Physics, Chinese Academy of Sciences, Beijing 100049, People's Republic of China;
- ⁴Institute of Space Sciences (ICE), CSIC, Barcelona E-08193, Spain;
- ⁵Institut d'Estudis Espacials de Catalunya (IEEC), Barcelona E-08034, Spain;
- ⁶Max Planck Institute for Extraterrestrial Physics, Garching 85748, Germany;
- ⁷Innovation Academy for Microsatellites, Chinese Academy of Sciences, Shanghai 201210, People's Republic of China;
- ⁸Department of Physics, University of Hong Kong, Hong Kong, People's Republic of China;
- ⁹School of Physics and Astronomy, University of Leicester, Leicester LE1 7RH, UK;
- ¹⁰School of Physics and Astronomy, Sun Yat-Sen University, Zhuhai 519082, People's Republic of China;
- ¹¹Department of Physics, Anhui Normal University, Wuhu 241002, People's Republic of China;
- ¹²Shanghai Institute of Technical Physics, Chinese Academy of Sciences, Shanghai 200083, People's Republic of China;
- ¹³Physics Department, Tsinghua University, Beijing 100084, People's Republic of China;
- ¹⁴Nevada Center for Astrophysics, University of Nevada Las Vegas, Las Vegas NV 89154, USA;
- ¹⁵Department of Physics and Astronomy, University of Nevada Las Vegas, Las Vegas NV 89154, USA;
- ¹⁶South African Astronomical Observatory, Cape Town 7935, South Africa;
- ¹⁷Department of Astronomy, University of Cape Town, Rondebosch 7701, South Africa;
- ¹⁸Department of Physics, University of the Free State, Bloemfontein 9300, South Africa;
- ¹⁹Université Paris Cité, CNRS, Astroparticule et Cosmologie, Paris F-75013, France;
- ²⁰Université Paris Cité, CEA Paris-Saclay, IRFU/DAP-AIM, Gif-sur-Yvette 91191, France;
- ²¹Department of Astronomy, Guangzhou University, Guangzhou 510006, People's Republic of China;
- ²²Cosmic Dawn Center (DAWN), Copenhagen 2200, Denmark;
- ²³Niels Bohr Institute, University of Copenhagen, Copenhagen 2200, Denmark;
- ²⁴Department of Physics and Astronomy, Rutgers, the State University of New Jersey, Piscataway NJ 08854-8019, USA;
- ²⁵Institute for Cosmic Ray Research, The University of Tokyo, Kashiwa City 277-8582, Japan;
- ²⁶ESA/ESTEC, Noordwijk 2201 AZ, The Netherlands;
- ²⁷Department of Astronomy, School of Physics, Huazhong University of Science and Technology, Wuhan 430074, People's Republic of China;
- ²⁸NAF – Osservatorio Astrofisico di Torino, Pino Torinese I-10025, Italy;
- ²⁹Sydney Institute for Astronomy, School of Physics A28, The University of Sydney, NSW 2006, Australia;
- ³⁰Department of Astronomy, Xiamen University, Xiamen 361005, People's Republic of China;
- ³¹Institute for Frontiers in Astronomy and Astrophysics, Beijing Normal University, Beijing 102206, People's Republic of China;
- ³²Department of Astronomy, University of Science and Technology, Hefei 230026, People's Republic of China;
- ³³School of Astronomy and Space Sciences, University of Science and Technology of China, Hefei 230026, People's Republic of China;
- ³⁴Institute of Deep Space Sciences, Deep Space Exploration Laboratory, Hefei 230026, People's Republic of China;
- ³⁵Department of Astronomy, School of Physics and Astronomy, Yunnan University, Kunming 650091, People's Republic of China;
- ³⁶Shanghai Astronomical Observatory, Chinese Academy of Sciences, Shanghai 200030, People's Republic of China;
- ³⁷Purple Mountain Observatory, Chinese Academy of Sciences, Nanjing 210023, People's Republic of China;
- ³⁸Key Laboratory for Research in Galaxies and Cosmology of Chinese Academy of Sciences, Department of Astronomy, University of Science and Technology of China, Hefei 230026, People's Republic of China;
- ³⁹Key Laboratory of Technology on Space Energy Conversion, Technical Institute of Physics and Chemistry, CAS, Beijing 100190, People's Republic of China;
- ⁴⁰North Night Vision Technology Co., LTD, Nanjing 210110, People's Republic of China;
- ⁴¹National Space Science Center, Chinese Academy of Sciences, Beijing 100190, People's Republic of China;
- ⁴²Institute of Electrical Engineering, Chinese Academy of Sciences, Beijing 100190, People's Republic of China;
- ⁴³Polar Research Institute of China, Shanghai 200136, People's Republic of China;
- ⁴⁴Key Laboratory for Polar Science, MNR, Polar Research Institute of China, Shanghai 200136, People's Republic of China

Received January 11, 2023; accepted April 6, 2023

We report the discovery of a peculiar X-ray transient, EP240408a, by *Einstein Probe* (*EP*) and follow-up studies made with *EP*, *Swift*, *NICER*, *GROND*, *ATCA* and other ground-based multiwavelength telescopes. The new transient was first detected with Wide-field X-ray Telescope (WXT) on board *EP* on April 8th, 2024, manifested in an intense yet brief X-ray flare lasting for 12 seconds. The flare reached a peak flux of 3.9×10^{-9} erg cm⁻² s⁻¹ in 0.5–4 keV, ~300 times brighter than the underlying X-ray emission detected throughout the observation. Rapid and more precise follow-up observations by *EP/FXT*, *Swift* and *NICER* confirmed the finding of this new transient. Its X-ray spectrum is non-thermal in 0.5–10 keV, with a power-law photon index varying within 1.8–2.5. The X-ray light curve shows a plateau lasting for ~4 days, followed by a steep decay till becoming undetectable ~10 days after the initial detection. Based on its temporal property and constraints from previous *EP* observations, an unusual timescale in the range of 7–23 days is found for EP240408a, which is intermediate between the commonly found fast and long-term transients. No counterparts have been found in optical and near-infrared, with the earliest observation at 17 hours after the initial X-ray detection, suggestive of intrinsically weak emission in these bands. We demonstrate that the remarkable properties of EP240408a are inconsistent with any of the transient types known so far, by comparison with, in particular, jetted tidal disruption events, gamma-ray bursts, X-ray binaries and fast blue optical transients. The nature of EP240408a thus remains an enigma. We suggest that EP240408a may represent a new type of transients with intermediate timescales of the order of ~10 days. The detection and follow-ups of more of such objects are essential for revealing their origin.

X-ray, transients, Einstein Probe**PACS number(s):** 98.70.Qy, 97.10.Gz, 97.60.Jd, 97.60.Lf**Citation:** W. Zhang, W. Yuan, Z. Ling, Y. Chen, N. Rea, A. Rau, et al, Einstein Probe discovery of EP240408a: a peculiar X-ray transient with an intermediate timescale, *Sci. China-Phys. Mech. Astron.* **66**, 000000 (2023), <https://doi.org/??>

1 Introduction

The X-ray sky is rich in variable and transient objects. Since the early days of X-ray astronomy, X-ray transients of diverse types have been found, and their variable or transient activities occur on a wide range of timescales spanning many orders or magnitude. In the long-timescale regime, the most well-studied X-ray transients are transient X-ray binaries (XRBs; also called X-ray novae) fuelled by accretion onto stellar-mass black holes or neutron stars, which occasionally enter outbursts that typically last months to a few years (see, e.g., refs. [1]); during the outbursts they exhibit strong variability over a large range of timescales down to as short as milliseconds. In recent years, a few dozens of X-ray transients associated with (mostly) the nuclei of galaxies lasting for from months to years have been found, which are interpreted as tidal disruption events (TDEs) where a star is disrupted and partially accreted onto a massive black hole [2-6]; in this process, strong gravity plays an important role in both the dynamics of the debris (essential for the early evolution of TDEs) and the X-ray emission (see refs. [7, 8] for a review).

On the other end of the spectrum, fast X-ray transients or intense short bursts with durations from sub-seconds to hundreds of seconds, and to hours have been found in large numbers for several decades (e.g. [9, 10]). Though being of heterogeneous origins, most of these events are believed to be produced in extremely violent processes on or involving stellar-mass objects. The most common examples are the X-ray counterparts or afterglows of gamma-ray bursts (GRBs) produced by collapse of massive stars or merger of two neutron stars [11], as well as X-ray flashes [12] that are thought to be the variants of GRBs. Others include flares from magnetars with ultrastrong magnetic fields [13, 14], supernova shock breakouts [15, 16], X-ray flares arising from coronal activities of stars lasting for mostly from within an hour to a day [17]. In recent years, samples of fast X-ray transients at fainter X-ray fluxes have also been found in deep X-ray surveys, some of unknown nature albeit with possible models suggested ([18, 19]), fast X-ray transients found in *Chandra* and *XMM-Newton* surveys, e.g. [20, 21].

In contrast, somewhere in between fast and long-term tran-

sients, X-ray transients with intermediate timescales appear to be comparably rarer, however. One interesting example in this timescale range is CXOU J005245.0-722844, a rare BeWD binary in the Small Magellanic Cloud, which entered a recent outburst lasting for only 6–12 days [22].

The *Einstein Probe (EP)* [23]¹⁾ is a space X-ray observatory dedicated to the discovery and characterization of X-ray transients. One of the two payloads onboard is the Wide-field X-ray Telescope (WXT), a soft X-ray focusing telescope with a ~ 3800 sq. deg. field-of-view (FoV) enabled by novel technology of lobster-eye micro-pore optics. Operating in the 0.5-4 keV band, WXT features a significantly improved sensitivity ($(2-3) \times 10^{-11}$ erg cm⁻² s⁻¹ at 1 ks exposure) over the current wide-field X-ray monitors, making it a powerful instrument in detecting relatively faint X-ray transients in soft X-rays. Another instrument is the Follow-up X-ray Telescope (FXT) [24] consisting of two co-aligned identical units using X-ray mirrors built from the Wolter-I optics and pn-CCDs as focal-plane detectors. FXT has a FoV of 1×1 square degrees, a spatial resolution of 20–24 arcsec (half-power diameter, on-axis) and an effective area of ~ 300 cm² at 1 keV (one unit). *EP* was launched on January 9th, 2024, followed by a commissioning and calibration phase of about 6 months. *EP* has started scientific operations since July, 2024.

On April 8th, 2024, a new X-ray transient, later dubbed EP240408a, was detected by *EP/WXT* in a calibration observation for FXT during the commissioning phase [25]. A series of follow-up observations with space- and ground-based telescopes at multi-wavelengths were triggered. In this work, we present the discovery, results of follow-up observations and discussion about the nature of this transient. The paper is organized as follows. In Section 2 we present the observations and the data reduction. The results are presented in Section 3. Based on the results, we discuss possible scenarios for the source in Section 4 and summarise our work in Section 5.

1) Einstein Probe is a international collaborative mission led by the Chinese Academy of Sciences and participated by ESA, MPE and CNES.

2 Observations and data reduction

On April 8th, 2024, an uncatalogued new X-ray source, designated EP240408a, was detected by EP/WXT during an observation in the commissioning phase [25]. We triggered prompt follow-up observations with the *Neil Gehrels Swift Observatory (Swift)* [26] and EP/FXT, ~ 33 and ~ 42 hours after the WXT detection, respectively. The source was further detected with much improved localization and spectral quality [27, 28] by both, the X-ray Telescope (XRT) [29] on board *Swift* and FXT; whilst no counterpart was detected in the optical to near-ultraviolet (NUV) band by the Ultra-Violet/Optical Telescope (UVOT) [30]. EP240408a was also observed with the *Neutron star Interior Composition Explorer (NICER)* [31] for several times, with the first observation carried out ~ 1.7 days after the WXT detection. The journal of the X-ray observations is given in Table 1. The source position was later observed with ground-based multi-wavelength telescopes in the optical, near-infrared (NIR) and radio bands, but no counterpart was detected, however. The observations and data reduction and analysis are presented in details in below.

2.1 Einstein Probe X-ray observations

2.1.1 EP/WXT

EP240408a was first detected on the CMOS sensor No. 29 of WXT in an observation (ObsID 13600005155) starting at April 8th, 2024 at 12:14:12 UT and lasting for 83.8 ks. The image is shown in the middle panel of Fig. 1, in which the source is clearly seen. The observation was divided into 20 segments due to Earth occultation and passage through the South Atlantic Anomaly (SAA), resulting in a net exposure of 38.5 ks. The WXT data are processed with `wxtpipeline`, an analysis chain of the WXT Data Analysis Software (WXTDAS) developed at the EP Science Center (EPSC). The `wxtpipeline` tool calibrates the raw data by performing coordinate transformation, flagging hot and bad pixels, computing the pulse invariant values, filtering the events to obtain a clean event list using the default criteria, and extracting a sky image from the clean event list. For the analysis, the events with grade patterns of 0–12 are selected. Then the tool carries out detection of point-like sources and extraction of the various products of detected sources, including the light curves and spectra, the ancillary response file and response matrix, as well as the background light curves and spectra. By default, the light curves and spectra of the sources are extracted from a circular region with a radius of $9.1'$, and those of the background are extracted from an annulus with inner and outer radii of $18.2'$ and $36.4'$, respectively.

In this observation, EP240408a was detected with a net count of 255.3 at a significance of 15.3σ in 0.5–4 keV. The WXT position of the source is R.A. = $10^{\text{h}}35^{\text{m}}23.9^{\text{s}}$, Decl. = $-35^{\circ}44'55''.2$ (J2000) with an uncertainty of $3'$ at the 90% confidence level (c.l.). There is no previously known X-ray source at this position, suggesting EP240408a to be a new X-ray transient. Thanks to the large field-of-view of WXT, several follow-up pointings covering the sky position of EP240408a were conducted, with exposure times ranging from 10.1 to 26.3 ks (see Table 1). The source was significantly detected till the observation taken on April 11th, 2024 (ObsID 08500000059). Since then EP240408a has remained no longer detected with WXT.

Since EP240408a was already present from the start of the discovery observation (ObsID 13600005155), it may have started to brighten before the observation. A search of the EP/WXT data at earlier epochs shows that the source position has been covered by WXT several times since March, 2024, at which no X-ray emission was detected, however. The latest observation (ObsID 08503145728) prior to the first detection was taken on March 26th, 2024 with an exposure time of 10.0 ks, imposing an upper limit of 2.6×10^{-3} counts s^{-1} (90% c.l.). The weakness of EP240408a is obvious by looking at the image extracted from this observation, as shown in the right panel of Fig. 1. Therefore, the onset of the transient is likely to occur sometime between March 26th and April 8th. Hereafter, we refer to the start of the first discovery observation, 2024-04-08UT12:14:12, as t_0 , the trigger time of EP240408a.

2.1.2 EP/FXT

The EP/FXT consists of two identical and co-aligned telescope units: FXT-A and FXT-B. FXT observed EP240408a twice (Table 1), with both FXT-A and FXT-B operating in the full-frame (FF) mode that has a time resolution of ≈ 50 ms. The first observation, beginning ~ 1.8 days (ObsID: 08500000058) after the initial detection by WXT, has an elapsed time of ~ 49 ks and an on-source time of ~ 24 ks, while the second observation (ObsID: 08500000116) was performed much later, on June 25th, 2024, with an exposure of 7.7 ks. The data are processed by using the `fxtchain` tool, as part of the FXT Data Analysis Software (FXTDAS) developed at the EPSC. This tool performs several tasks, including identifying particle events, calculating pulse-invariant values for the event files, flagging bad and hot pixels in the FXT detectors, and selecting good time intervals using housekeeping data. It then extracts the spectra and light curves for both the source and background, and produces ancillary files and redistribution matrices.

In the first FXT observation, an X-ray source was detected

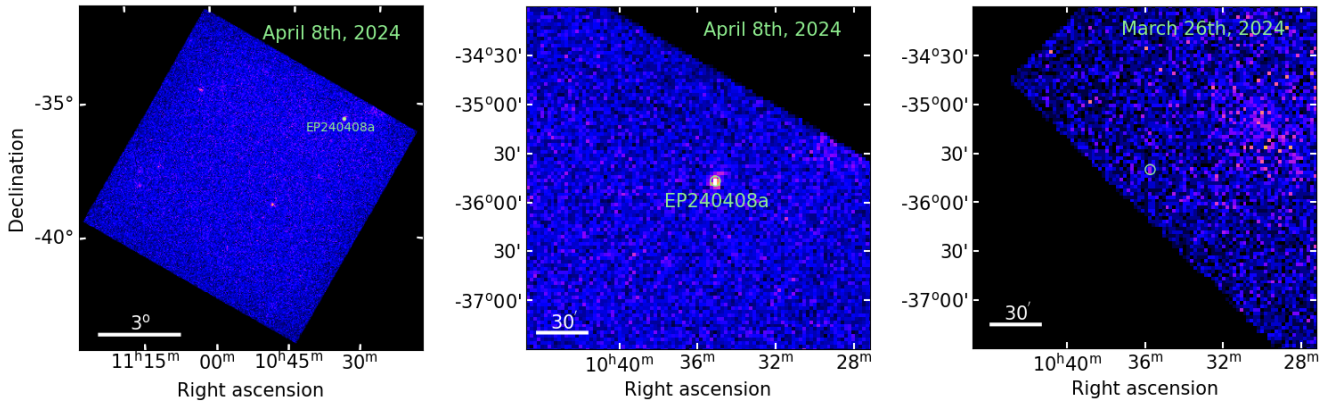


Figure 1 Discovery X-ray images of EP240408a in 0.5–4 keV obtained with *EP/WXT*: on the whole CMOS detector chip (left) and a close-up (middle). An X-ray image at the source position extracted from an observation taken ~ 13 days before the discovery is also shown for comparison (right). In all panels, the WXT error circle of 3 arcmin in radius is marked by a green circle at the position of EP240408a.

within the WXT positional error circle of $3'$ (90% c.l.), suggestive of being consistent with the WXT source. The FXT observation also improves significantly the source localization, reaching a precision of 5 arcsec (90% c.l.). The images of the FXT detection are shown in Fig. 2. The net source count is 2.4×10^4 for FXT-A and 2.7×10^4 for FXT-B, giving a source count rate of $0.94 \text{ counts s}^{-1}$ and $1.05 \text{ counts s}^{-1}$, respectively. The source was not detected in the second FXT observation taken on June 25th, 2024, setting a 3σ upper limit on the source count rate as $1.84 \times 10^{-3} \text{ counts s}^{-1}$ in 0.5–10 keV.

2.2 *Swift* observations in X-ray, optical and UV

The *Swift* observatory observed EP240408a five times from April 10th to April 27th (PI: Jingwei Hu; see Table 1), with the first observation taken ~ 33 hours after the initial WXT detection. For all the observations, the *Swift*/XRT was configured in the photon counting (PC) mode. During the first observation on April 10th, an X-ray source was detected at a position consistent with that of the FXT source (thus within the WXT error circle, see Fig. 2), suggesting its association with EP240408a. The XRT observation gives a further improved source position, enhanced by applying correction using the *Swift*/UVOT astrometry [32]: R.A. = $10^{\text{h}}35^{\text{m}}23^{\text{s}}.96$, Decl. = $-35^{\circ}44'55''.1$ (J2000; uncertainty of $2.2''$ at the 90% c.l.)²⁾. The FXT source position is well consistent with the XRT position (marked as a red cross in Fig. 2), with a separation of only 0.7 arcsec, though its uncertainty of $\sim 5''$ is slightly larger. We thus adopt the XRT coordinates as the X-ray position of EP240408a.

The light curves and spectra are extracted from a circular aperture with a radius of 47.2 arcsec for the source, and an annular region with inner and outer radii of 94.4 and 188.8 arcsec, respectively, for the background. In this observation, the source has a total of 654.5 net source counts and an averaged count rate of $0.36 \pm 0.01 \text{ counts s}^{-1}$ in 0.5–10 keV. In the following four observations, EP240408a was no longer detected by XRT. We derive 3σ upper limits on the net source count rate ranging from 0.005 to 0.01 counts s^{-1} (0.5–10 keV), depending on the duration of the observation. By combining the data from these observations, a more stringent upper limit of $0.003 \text{ counts s}^{-1}$ (0.5–10 keV) are set.

During the first observation, the *Swift*/UVOT operated in the image mode and utilized all six of its filters. EP240408a was not detected in any of these filters, however, down to the following magnitude limits (the Vega system): UVW2 > 19.5 mag, UVM2 > 18.9 mag, UVW1 > 18.6 mag, U > 19.4 mag, B > 19.8 mag, V > 18.9 mag.

2.3 *NICER* X-ray observations

The X-ray Timing Instrument (XTI) onboard *NICER* observed EP240408a 32 times (PIs: Nanda Rea, Brendan O'Connor), first beginning on April 10th at 18:30:31 UT, ~ 41 hours after the initial WXT detection. The data are processed using *nicer12* with specific options *overonly_range* = 0–5 and *cor_range* = "1.5–*", to minimize potential contamination from non-X-ray flares³⁾. After applying such a strict selection criterion, only 6 out of the first 12 observations (7204340101–7204340112) are left with clean events. From the observation on April 22nd (ObsID 7204340113) onward,

2) In the GCN reporting the XRT observation [27], the XRT localization was reported without correction using the UVOT astrometry. The new XRT position is now $5.5''$ away from the position that was reported in that GCN.

3) https://heasarc.gsfc.nasa.gov/docs/nicer/analysis_threads/flares/

Table 1 Journal of the X-ray observations of EP240408a presented in this work.

Telescope/Instrument (Mode)	Obs ID	Start – End time	Exposure (ks)
		Mmm DD hh:mm:ss (UTC)	
EP/WXT-29	13600005155	Apr 8 12:14:12 – Apr 8 11:44:06	38.5
Swift/XRT (PC)	00016599001	Apr 10 02:57:40 – Apr 10 04:48:35	1.8
EP/WXT-14	08500000058	Apr 10 12:30:12 – Apr 11 04:00:54	26.2
EP/WXT-37	08500000058	Apr 10 12:30:12 – Apr 11 04:00:54	26.3
EP/FXT (FF)	08500000058	Apr 10 12:36:18 – Apr 11 02:17:06	24.0
NICER/XTI	7204340101	Apr 10 18:30:31 – Apr 10 21:40:18	0.3
NICER/XTI	7204340102	Apr 11 02:08:20 – Apr 11 02:18:54	0.5
EP/WXT-13	08500000059	Apr 11 20:35:44 – Apr 12 08:06:03	14.4
EP/WXT-38	08500000059	Apr 11 20:35:44 – Apr 12 08:06:03	10.1
NICER/XTI	7204340103	Apr 12 09:07:29 – Apr 12 18:51:20	2.0
NICER/XTI	7204340104	Apr 13 00:49:45 – Apr 13 20:51:00	1.4
NICER/XTI	7204340105	Apr 14 04:29:47 – Apr 14 12:16:01	0.3
NICER/XTI	7204340106	Apr 15 08:22:22 – Apr 15 08:29:54	0.5
Swift/XRT (PC)	00016599003	Apr 19 03:41:27 – Apr 20 03:27:53	1.0
Swift/XRT (PC)	00016599004	Apr 21 03:03:55 – Apr 21 04:50:52	1.2
NICER/XTI	7204340113	Apr 22 01:22:59 – Apr 22 01:27:45	0.3
Swift/XRT (PC)	00016599005	Apr 24 03:53:46 – Apr 24 10:04:52	1.0
Swift/XRT (PC)	00016599006	Apr 26 04:40:59 – Apr 27 07:31:52	2.4
EP/FXT (FF)	08500000116	Jun 25 07:07:09 – Jun 25 10:54:29	7.7

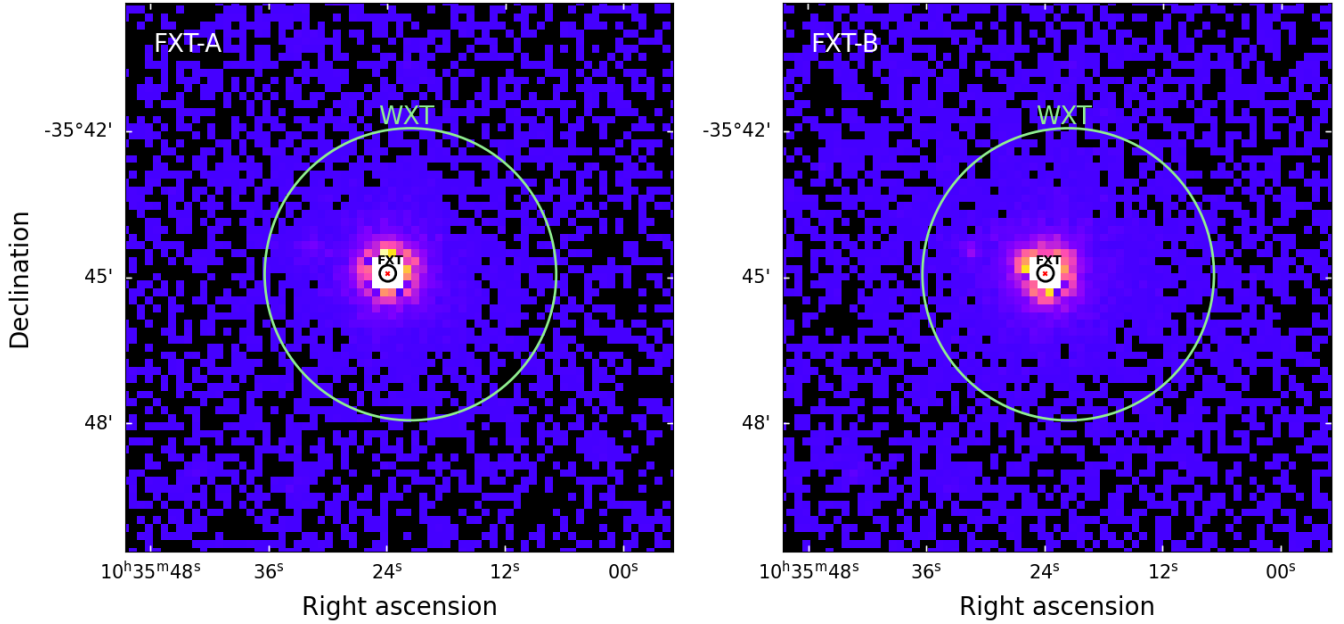


Figure 2 X-ray images of EP240408a obtained with the two EP-FXT units, FXT-A (left) and FXT-B (right), extracted from the observation taken ~ 42 hours after the discovery by WXT. The WXT and FXT localizations are indicated by green and black circles, respectively, while the XRT position with an error radius of $2.2''$ is indicated by a red cross.

the source was no longer detected with XTI. For brevity, only the NICER observations where EP240408a is detected are listed in Table 1.

The photon arrival times are corrected to the barycenter of the Solar system using the XRT position and the JPL DE430 ephemeris. Light curves and spectra are extracted using the `nicer13-1c` and `nicer13-spec` pipelines, respectively, employing the SCORPEON background model⁴). For spectral fitting, we fit the source and background spectra jointly in the energy range of 0.5–12 keV, with the background model parameters `niscorpv23_noisenorm`, `niscorpv23_skyllhb_em` and `niscorpv23_skygal_nh` fixed. The background parameter `niscorpv23_swxcok_norm` is left free to vary if an excess towards low energies is seen around ~ 0.6 keV, to model the oxygen $K\alpha$ emission by the solar wind.

2.4 Upper limits from other high-energy missions

eROSITA: The position of EP240408a was covered by eROSITA [33] on board the Spektrum Roentgen Gamma observatory for ~ 127 s during the first six months of survey operations [34]. No X-ray emission was detected at the source position, with a flux upper limit of 6×10^{-14} erg cm $^{-2}$ s $^{-1}$ (0.2–2.3 keV; see refs. [35]).

GECAM: The Gravitational wave high-energy Electromagnetic Counterpart All-sky Monitor (GECAM) is a GRB monitor operating in the hard X-ray to gamma-ray band, consisting of two identical micro-satellites in opposite orbital phases [36]. One of the satellite modules, GECAM-B, covered the sky position of EP240408a at the time of the first WXT detection [37]. No sources were detected and upper limits of $\sim (2-4) \times 10^{-6}$ erg cm $^{-2}$ were imposed on the 15–300 keV fluence, varying with the spectral model assumed. The fluence is integrated with respect to the time interval of the soft X-ray flare detected in the WXT light curve of EP240408a during the first-detection observation (see below).

2.5 Optical and near-infrared observations

Follow-up observations were carried out with the *Gamma-Ray Burst Optical Near-ir Detector (GROND)* [38] instrument mounted on the MPG 2.2m telescope at ESO's La Silla Observatory on April 10th, 12th, 17th and May 27th, 2024. These observations were performed simultaneously in the J, H, and K $_s$ -bands with typical exposures of 30 min per epoch and band. The data are reduced using the standard IRAF-based GROND pipeline [39]. The aperture photometry is

4) https://heasarc.gsfc.nasa.gov/docs/nicer/analysis_threads/scorpeon-overview/

calibrated against the Two Micron All Sky Survey catalogue (2MASS) [40] and converted into the AB magnitude system. No NIR source was found in the GROND images within the *Swift*/XRT error circle down to 3σ limiting AB magnitudes of $J > 21.4$, $H > 21.2$, and $K_s > 19.6$. An unresolved source is detected in the J and H-bands at R.A. = $10^{\text{h}}35^{\text{m}}24^{\text{s}}.31$, Decl. = $-35^{\circ}44'47''.8$ (J2000) with an uncertainty of $0.16''$ and $0.13''$, respectively (source A in Fig. 3). This source was initially suggested to be the counterpart to EP240408a by refs. [41], but it is now located $8.0''$ from the centre of the enhanced $2.2''$ radius XRT error circle.

In addition, several other optical observations were conducted, but none detected an optical counterpart. Observations made with GSP, MASTER and BOOTES-6/DPRT yielded upper limits of 21.5 mag in the r-band [42], 19.5 mag (unfiltered) [43], and 20.5 mag (clear filter) [44], taken ~ 17 hours, ~ 23 hours, and ~ 25 hours after the initial X-ray detection, respectively. The 2.56 m Nordic Optical Telescope (NOT; Roque de los Muchachos observatory, La Palma, Spain) performed late time observations on April 17th, 18th, and May 2nd (9.2, 10.2, and 24.1 days after the initial X-ray detection), obtaining upper limits of 20.8, 21.4, and 22.0 mag, respectively, in the z-band.

2.6 ATCA radio observations

We observed EP240408a with the *Australia Telescope Compact Array* (ATCA) on May 8th and 10th, 2024, ~ 30 and ~ 32 days after the initial X-ray detection respectively, under the Director's Discretionary Time program with code CX570 (PI: Xinwen Shu). The observations were first performed at the C-band and then at the K-band, using dual receivers with central frequencies of 5.5/9, and 16.7/21.2 GHz, respectively. All observations were taken with the ATCA CABB in the full 2048 spectral channel mode, resulting in 2 GHz of bandwidth. To solve for the time-dependent complex gains, we used the nearby phase calibration source 1034-374 for C-band and 1048-313 for K-band, while the standard calibrators 0823-500 and 1034-293 were used as bandpass calibrators and to set flux density scale for C-band and K-band, respectively.

The data are reduced using the Common Astronomy Software Applications (CASA, version 5.6.1)[45]. By loading the data using the IMPORTATCA task, we examine each spectral window and flagged abnormal data due to the radio frequency interference or hardware issues. After checking and flagging the data, we set the flux scale for the bandpass calibrator using the `setjy` task. Finally, we calibrate the data and then apply the solutions to EP240408a. The calibrated data are then selected and we employ the CLEAN algorithm to remove possible contamination from side-lobes, utilizing

the conventional Briggs weighting with a ROBUST parameter of 0.5. The final cleaned maps exhibit an rms noise of $\sim 25 \mu\text{Jy/beam}$ in the C-band and $\sim 40 \mu\text{Jy/beam}$ in the K-band, measured using the IMFIT task in CASA. We do not detect EP240408a in either C-band or K-band, resulting in 5σ upper limits of $\sim 125 \mu\text{Jy}$ and $\sim 200 \mu\text{Jy}$ on the flux density, respectively.

3 Observed properties of EP240408a

EP240408a is positioned at R.A. = $10^{\text{h}}35^{\text{m}}23^{\text{s}}.96$, Dec. = $-35^{\circ}44'55''.1$ (J2000; uncertainty of $2.2''$ at 90% c.l.), determined by *Swift*/XRT and consistent with the *EP*/FXT measurement. No counterparts were detected in the other wavebands observed, however. This section presents the X-ray temporal and spectral properties of EP240408a, ending with a summary of the observed properties.

3.1 X-ray temporal property

3.1.1 Short-term X-ray flare

Fig. 4 shows the X-ray light curve of EP240408a in 0.5–4 keV obtained during the *EP*/WXT observation (ObsID 13600005155) in which the transient was first detected. The overall light curve (upper panel in Fig. 4) spans over the length of the observation of 83.8 ks, with time bins corresponding to the (orbital) segments. Of particular interest, a short-term yet intense flare with a duration of ~ 10 s occurred clearly at an epoch ~ 19.8 ks from the start of the observation, as shown in a close-up light curve of the 4th segment with a bin size of 30 s (lower panel in Fig. 4). To study the flare in detail, we extract photon event lists of the source and background from the time segment in which the flare is located, and apply the Bayesian Block (BB) [46] algorithm to the event lists. As the background is also variable, in practice we utilize a modified version of the BB algorithm introduced by refs. [47], which accounts for the variation of the background. The start time and the duration of the flare, as determined by the BB algorithm are 2024-04-08UT17:44:54.9 and 12.3 s, respectively. The average net count rate during the flare is $1.57 \text{ counts s}^{-1}$, which is over two orders of magnitude higher than the persistent count rate of $6.78 \times 10^{-3} \text{ counts s}^{-1}$. A light curve of the flare with an even finer bin size of 1 s is extracted and shown in the inset of the lower panel of Fig. 4. It shows that the flare possibly exhibits three peaks, each having a largely symmetric profile.

We find that the source was already significantly detected above the background even *before* the short-term flare. In fact, apart from the flare, the source did not show significant variation in 0.5–4 keV during the overall observation of

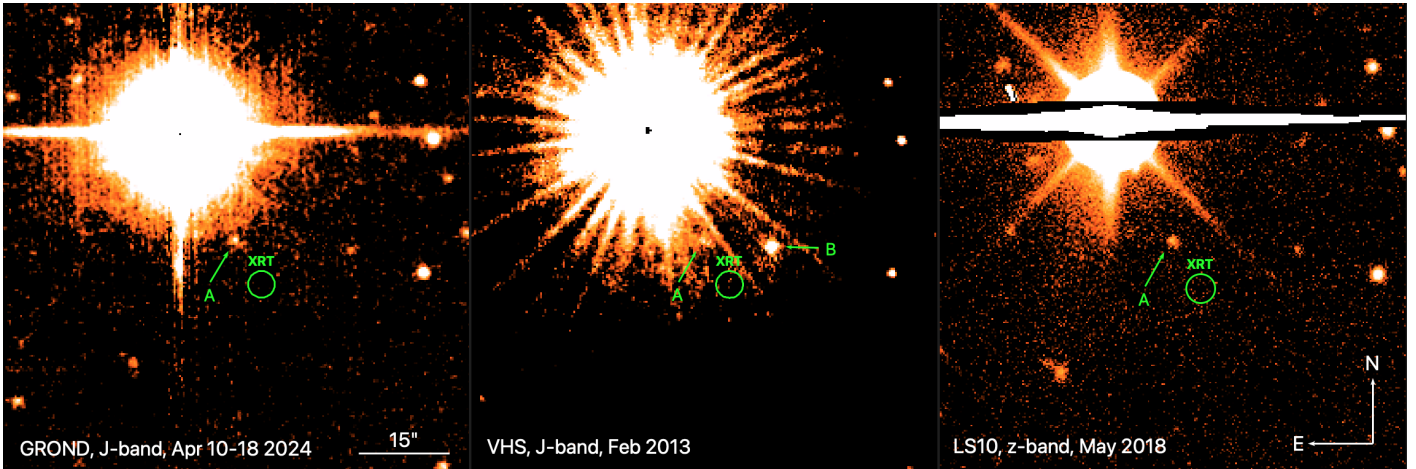


Figure 3 *Left:* GROND J-band stack of the best-seeing data from April 10th, 12th, and 18th, 2024. A faint source (marked A) is detected 8.0'' from the centre of the 2.2'' radius *Swift*/XRT error circle (the green circle). *Middle:* Archival J-band image from the VISTA Hemisphere Survey (VHS) obtained in Feb 2013 showing emission consistent with source A. *Right:* Archival Legacy Survey DR10 (LS10) z-band image taken in May 2018 also showing source A. Note, there is a bright source, B, $\sim 9.3''$ to the West of the XRT position seen in the VHS data. No source is detected at this position by GROND and LS10.

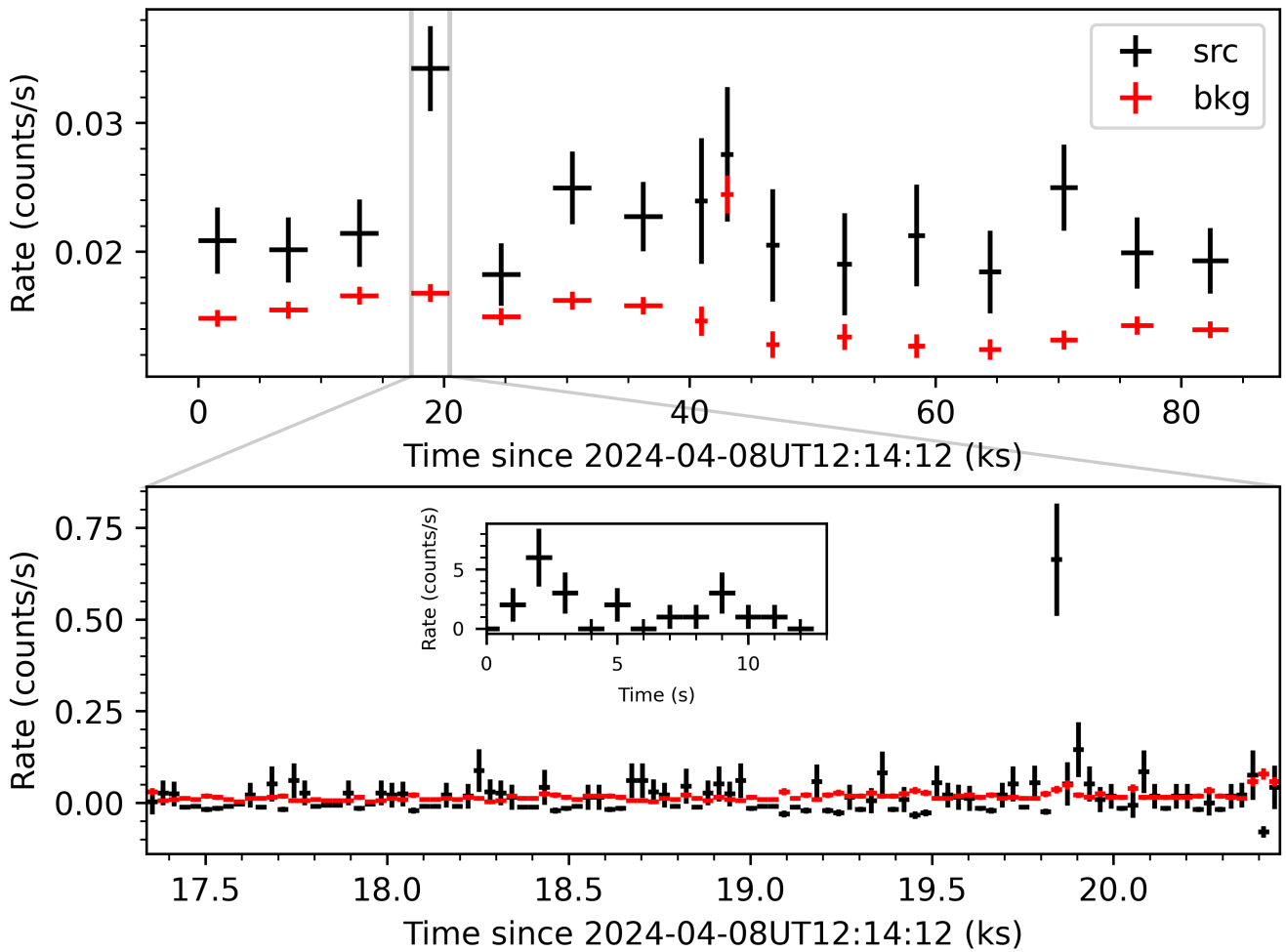


Figure 4 Light curves of EP240408a of the WXT observation (13600005155) in which the transient was initially detected. Upper panel: the light curve of the entire observation. The background light curve (red) is also plotted for comparison. The time bins correspond to the orbital segments of the observation. For a few segments with a short duration, their light curves are not shown for clarity. Lower panel: a detailed light curve of the 4th segment, in which the short-term flare is located. The temporal bin size is 30 s. The inset shows the detailed light curve of the flare with a temporal bin size of 1 s.

83.8 ks. No similar flares are found in the light curves of the other X-ray observations of EP240408a.

3.1.2 Overall X-ray light curve

EP240408a was detected by *EP/WXT* and *NICER/XTI* multiple times, with *WXT* covering the early part and *XTI* covering the latter part of the observations. We demonstrate the variation of its X-ray emission in a model-independent approach by using the count rates and spectral hardness measured by each of the two instruments, respectively. Light curves are extracted in two energy bands, a soft (0.5–1 keV) and a hard band (1–4 keV for *EP/WXT* and 1–5 keV for *NICER/XTI*). The choice of the dividing energy at 1 keV is somewhat operational, so as to give roughly comparable numbers of counts in the two bands. We define hardness ratio as $(H - S)/(H + S)$, where S and H denote the *background-subtracted* count rates in the soft and hard bands, respectively.

We present the results from the *EP/WXT* observations in Fig. 5 (right panel) and those from *NICER/XTI* in Fig. 6. Overall, the evolution of the count rates shows little variation from the beginning up to ~3–4 days later, followed by a fast drop down to a level that is one order of magnitude lower around day 6. Interestingly, the count rate shows somewhat increase again on day 7 as measured by *NICER* (ObsID 7204340106). EP240408a was further monitored with *Swift/XRT* and *NICER/XTI* later in April, 2024; no X-ray emission has been detected ever since, however, indicating that its X-ray emission has likely faded away.

The spectral shape exhibits a gradual and slight hardening over time until day 5, thereafter followed by spectral softening within the next day, up to day 6. However, the uncertainties are too large to draw a firm conclusion.

We also present intra-observation count rates and hardness ratios during the *WXT* observation of the initial source detection (left panel in Fig. 5). The observation is divided into three epochs: pre-flare, flare, and post-flare, with the flare's time interval determined by the BB algorithm, as described in Sec. 3.1. The count rate of the flare is more than two orders of magnitude larger than the persistent level, whereas the hardness ratio of the flare is statistically consistent with that of the persistent emission. The result also confirms the aforementioned finding that X-ray emission from the source was already present even prior to the short-term flare.

3.2 X-ray spectral property

Here we present the analysis of the X-ray spectra of EP240408a, based on the data acquired by *EP*, *NICER* and *Swift*, as reduced in Sec. 2. For the *XRT* and *FXT* spectra, the

energy band of 0.5–10 keV is selected, while the 0.5–4 keV band is used for *WXT*. For the *XTI* spectra, a broader energy band of 0.5–12 keV is employed to better constrain the *XTI* background component. We perform X-ray spectral fitting with *Xspec* [48] v12.14.1. We group all the spectra with a minimum of 3 counts in each bin and the best fit is found by minimizing the Cash statistics [49], given the low number of counts of *XTI* above ~10 keV. The *wilms* abundance table [50] is used. The spectra are fit with three simple models: an absorbed power-law model (*tbabs * powerlaw* in *Xspec*), an absorbed thermal blackbody model (*tbabs * bbody*) and an absorbed disk blackbody model (*tbabs * diskbb*). All uncertainties derived from the spectral fitting are reported at the 90% confidence level.

We begin by performing a joint fit of the *FXT* spectra (ObsId 08500000058) and the *NICER* spectrum (ObsId 7204340101), which were observed quasi-simultaneously. This results in joint energy spectra of the best quality among all the X-ray observations available for EP240408a. Exclusively for the joint fit, we add a multiplicative constant as a scaling factor of the normalization parameter to account for calibration uncertainties between different instruments. The inter-calibration constant C is fixed to unity for *FXT-A*, while it is allowed to vary for *FXT-B* and *XTI*.

A power-law model provides an acceptable fit, yielding a $cstat$ value of 1246.28 with 1147 degrees of freedom (dof). The energy spectra and the best-fit model are presented in Fig. 7. In this model, the inter-calibration constant is 0.97 ± 0.01 for *FXT-B* and $1.07^{+0.06}_{-0.04}$ for *XTI*, demonstrating consistency of the calibration across these instruments. The best-fit power-law photon index is $\Gamma = 2.10 \pm 0.03$, and the hydrogen column density, that accounts for interstellar absorption along the line of sight (*tbabs*), is $N_H = (1.6 \pm 0.1) \times 10^{21} \text{ cm}^{-2}$. For comparison, the N_H in this direction obtained from the neutral hydrogen HI4PI HI survey [51] is $6.2 \times 10^{20} \text{ cm}^{-2}$. The best-fit parameters are summarized in Table 2. However, an absorbed thermal model, either blackbody or disk blackbody, does not provide an acceptable fit ($cstat/dof = 9679.10/1148$ and $2550.11/1148$, respectively). We thus conclude that the X-ray radiation of EP240408a is of non-thermal origin.

Then, we proceed to fit the remaining spectra with the absorbed power-law model exclusively. In fitting the *WXT* and *XTI* spectra, we find the N_H value to be poorly constrained, so we fix it at the best-fit value of $1.6 \times 10^{21} \text{ cm}^{-2}$, derived from the joint fit. For the *XRT* spectrum, the N_H value is freely fitted, resulting in a best-fit value of $(1.5 \pm 0.4) \times 10^{21} \text{ cm}^{-2}$, which is consistent with the value obtained from the joint fit of the *FXT* and *XTI* spectra. A simple absorbed power-law model provides acceptable fits across all the remaining spectra, with $cstat/dof$ values ranging between 0.8 and 1.2. The fitted parameters are presented in Table 2.

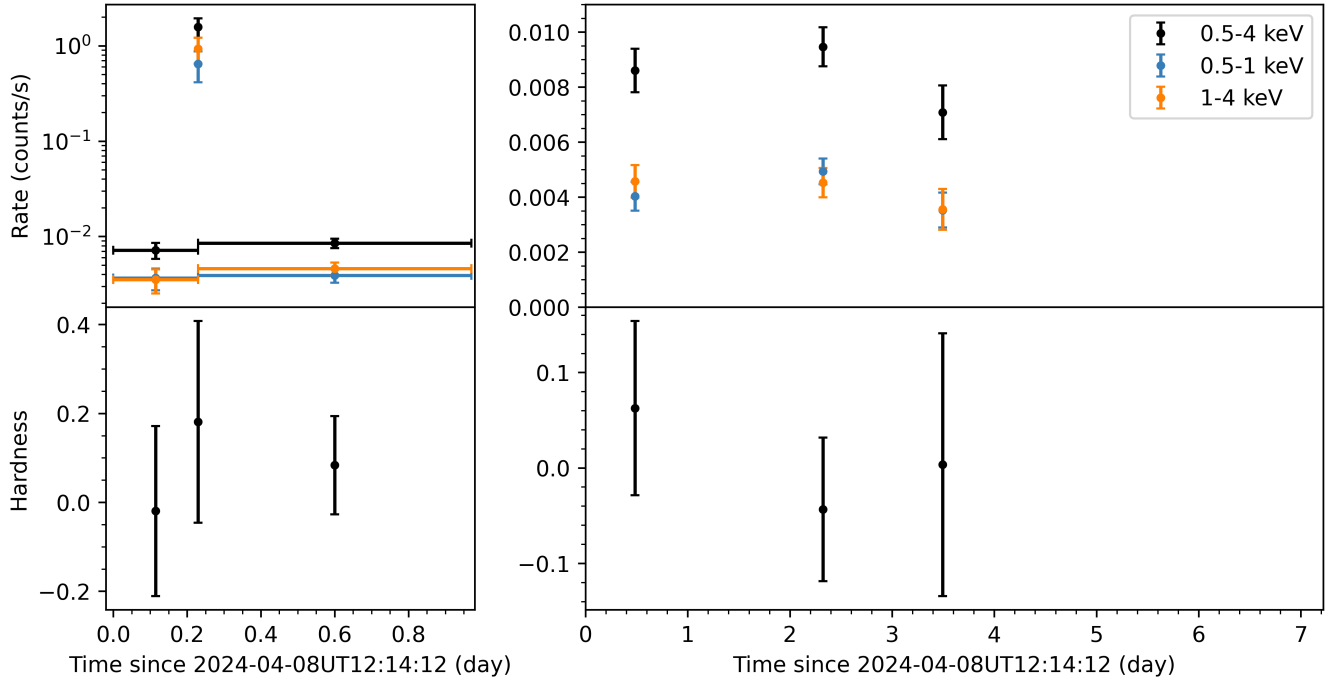


Figure 5 Left: the averaged count rates (upper) and hardness ratios (lower) in the pre-flare, flare and post-flare epochs during the first WXT observation. Right: averaged count rates (upper) and hardness ratio (lower) for the 3 WXT observations. Light curves of the soft (0.5–1 keV; orange) and hard (1–4 keV; blue) bands are shown.

We also fit the WXT spectrum of the short-term X-ray flare, which was extracted from the time interval of the flare (12.3 seconds) derived above in the WXT observation (ObsID 13600005155). The spectral shape cannot be constrained due to limited source counts. Interesting enough, the flare reaches a flux of a few times 10^{-9} erg cm $^{-2}$ s $^{-1}$, 300 times the averaged value of the persistent emission before and after the flare. The measured fluence of the flare is $5^{+12}_{-2} \times 10^{-8}$ erg cm $^{-2}$.

3.3 Evolution of the X-ray emission

The temporal evolution of the best-fit values of the X-ray flux and power-law photon index is presented in Fig. 8 on logarithmic scales. To keep consistent with the WXT energy band, we report the fluxes in the 0.5–4 keV band for all instruments. Initially, the average X-ray flux, around 10^{-11} erg cm $^{-2}$ s $^{-1}$, appears to remain in a plateau phase with little or no decrease for ~ 3 –4 days. This is followed by a steep decay to a flux level of $\sim 10^{-12}$ erg cm $^{-2}$ s $^{-1}$ around day 6–7. Afterward, EP240408a was no longer detected in X-rays during several *Swift*/XRT observations taken ~ 10 days after the initial WXT detection. We obtain 3σ upper limits on the count rate at the source position utilizing `ximage` in the `FTOOLS` package, corresponding to flux limits of a

few times 10^{-13} erg cm $^{-2}$ s $^{-1}$ in 0.5–4 keV. The flux limits are derived from the count rate to flux conversion using `WebPIMMS`⁵⁾, assuming an absorbed power-law model with $N_{\text{H}} = 1.6 \times 10^{21}$ cm $^{-2}$ and $\Gamma = 2$. The upper limits set by *Swift*/XRT are consistent with the steep decline in flux observed by *NICER*/XTI. We also derive a 3σ upper limit on the flux in 0.5–4 keV of 1.97×10^{-14} erg cm $^{-2}$ s $^{-1}$ for the second FXT observation taken on June 25th, based on the upper limits on the count rate (see Sec. 2) and the conversion factor from spectral fitting.

We parameterize the 0.5–4 keV flux (excluding upper limits) as a function of time since t_0 with a few phenomenological models. Fitting a broken power-law model to the data indicates that the shallow and steep decay phases are best described by $t^{-0.3}$ and $t^{-5.5}$, respectively, with the transition occurring at $t \sim 4.6$ days after trigger. The best-fit model is represented by a solid gray line in the upper panel of Fig. 8. As can be seen in the figure, while the XRT upper limits are not included in the fit, the best-fit broken power-law model is well consistent with the upper limits. The decay index of the shallow decay phase is close to 0, consistent with being a plateau phase. We experiment with fixing the index in the steep decay phase of the broken power-law at $-5/3$, the canonical TDE decay rate, and find the late-time emission to be obviously over-estimated (dash-dotted gray line). Al-

5) https://heasarc.gsfc.nasa.gov/Tools/w3pimms_help.html

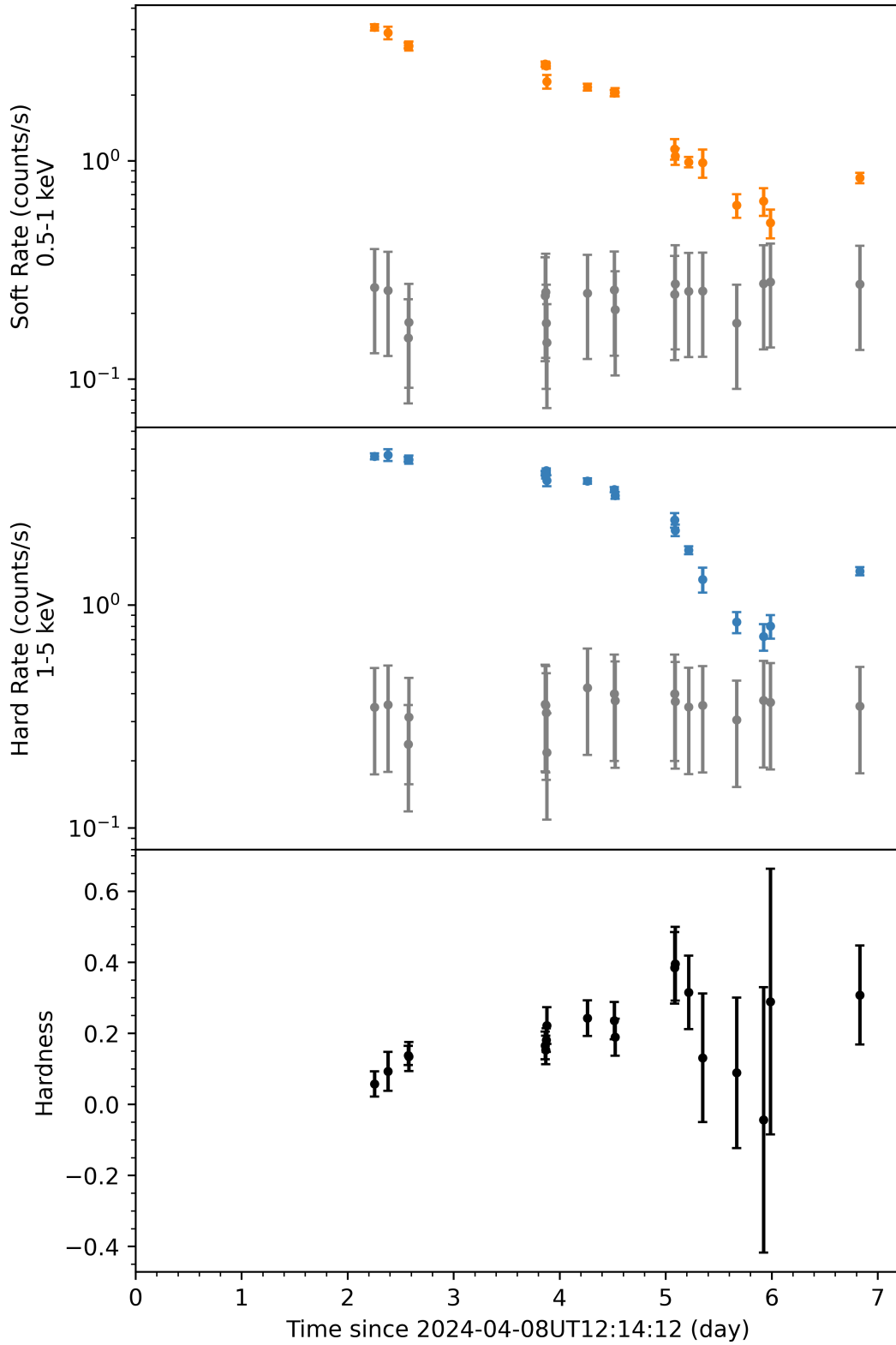


Figure 6 NICER light curve of EP240408a. The total count rates (i.e. without background subtraction) of the soft (0.5–1) and hard (1–5 keV) bands are plotted in the upper and middle panels, respectively. In both panels, the background count rate in the respective band estimated with the SCORPEON model is plotted in gray dots. The hardness, defined as $(H - S)/(H + S)$ where H and S are the *net* count rates of the soft and hard bands, respectively, is presented in the bottom panel.

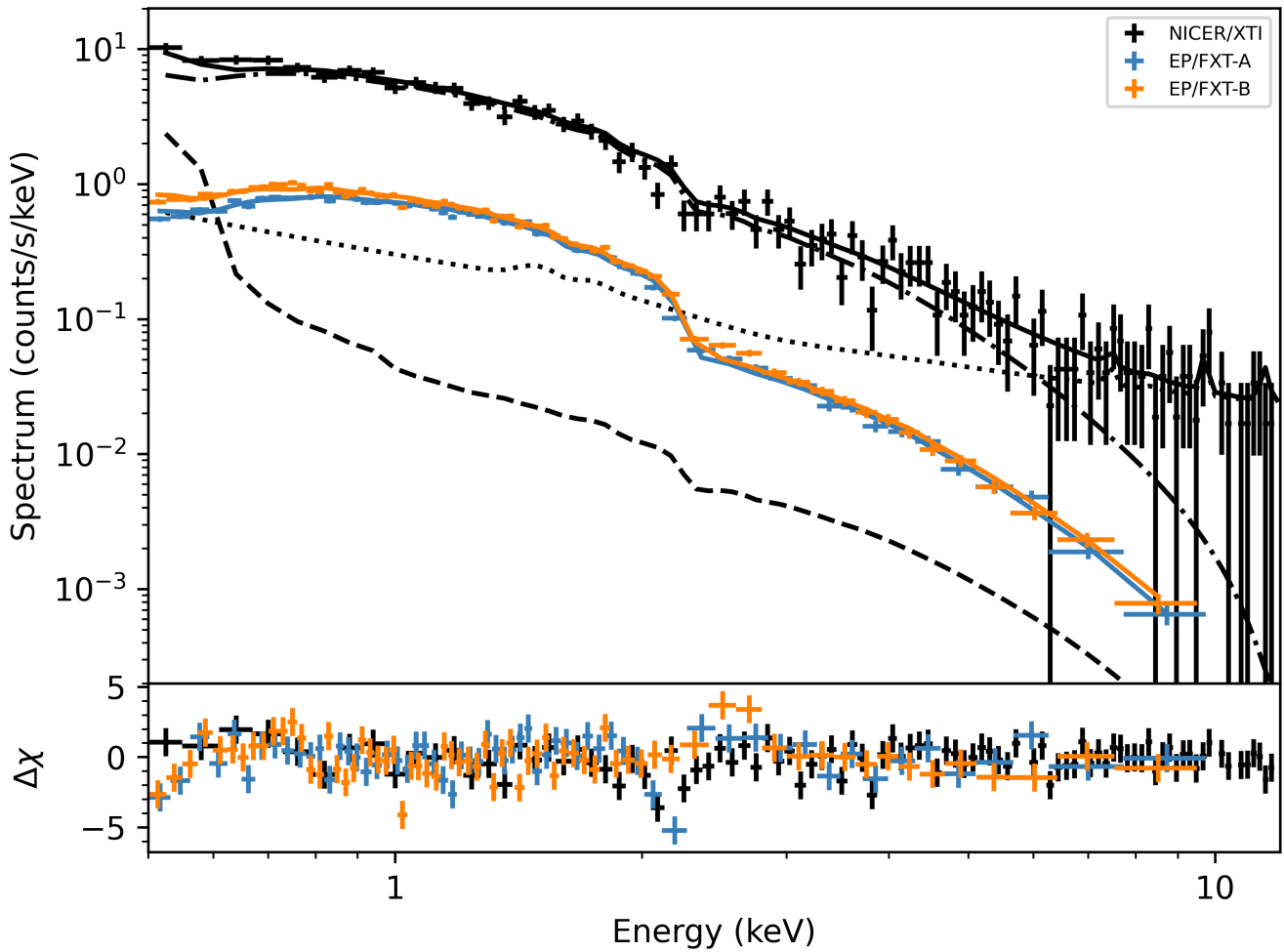


Figure 7 Upper: the energy spectra and the best-fit model for the joint XTI/FXT fit. The results of XTI, FXT-A, FXT-B are plotted in black, blue, and orange colors, respectively. The spectra of FXT-A and FXT-B are rebinned for clarity. For each instrument, the spectrum is represented by the crosses, while the best-fit model is plotted in a solid curve. For XTI, the source, sky background, and non-X-ray background models are plotted in dash-dotted, dashed, and dotted lines, respectively. Lower: $\Delta\chi$, defined as $(data - model)/error$. The residuals around ~ 2.2 keV for both XTI and FXT-A are probably due to imperfect calibrations of instrumental gold edges.

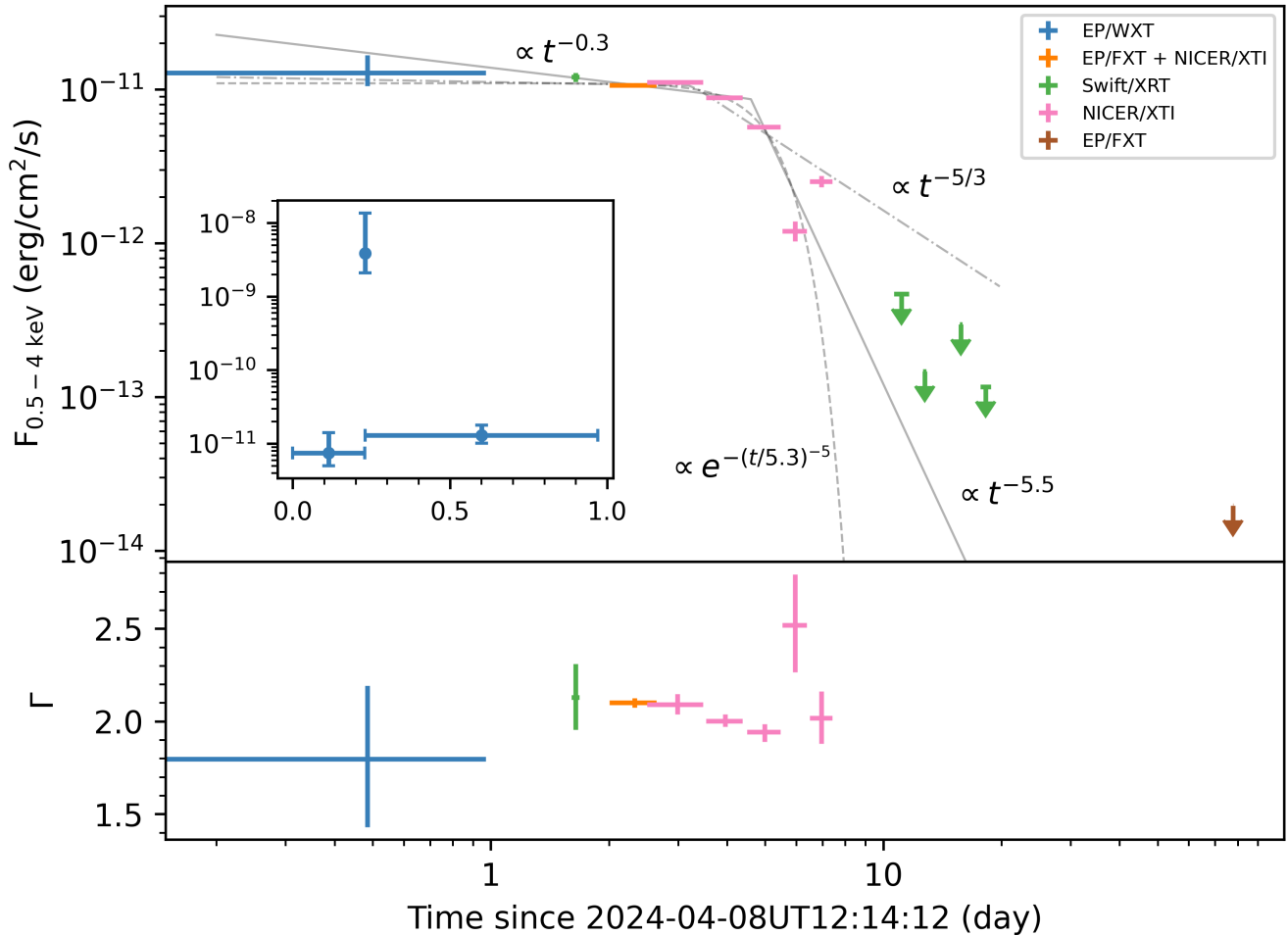


Figure 8 X-ray spectral evolution of EP240408a. In the upper and lower panels, we present, as a function of time, the 0.5–4 keV flux and the photon index, respectively. Results from various instruments are plotted in different colors, as indicated in the plot. The upper limits on the flux by *Swift*/XRT observations taken after day 10 are plotted with green arrows, and the upper limit on the flux by the second FXT observation taken on June 25th is plotted with a brown arrow. In the inset plot of the upper panel, we also present the evolution of the flux within the first WXT observation. Gray curves represent phenomenological fits to the flux evolution: the best-fit broken power-law, and modified exponential decay (see text) are plotted in solid and dashed lines, respectively. The dash-dotted line represents the best-fit broken power-law model with the index after the break fixed at $-5/3$.

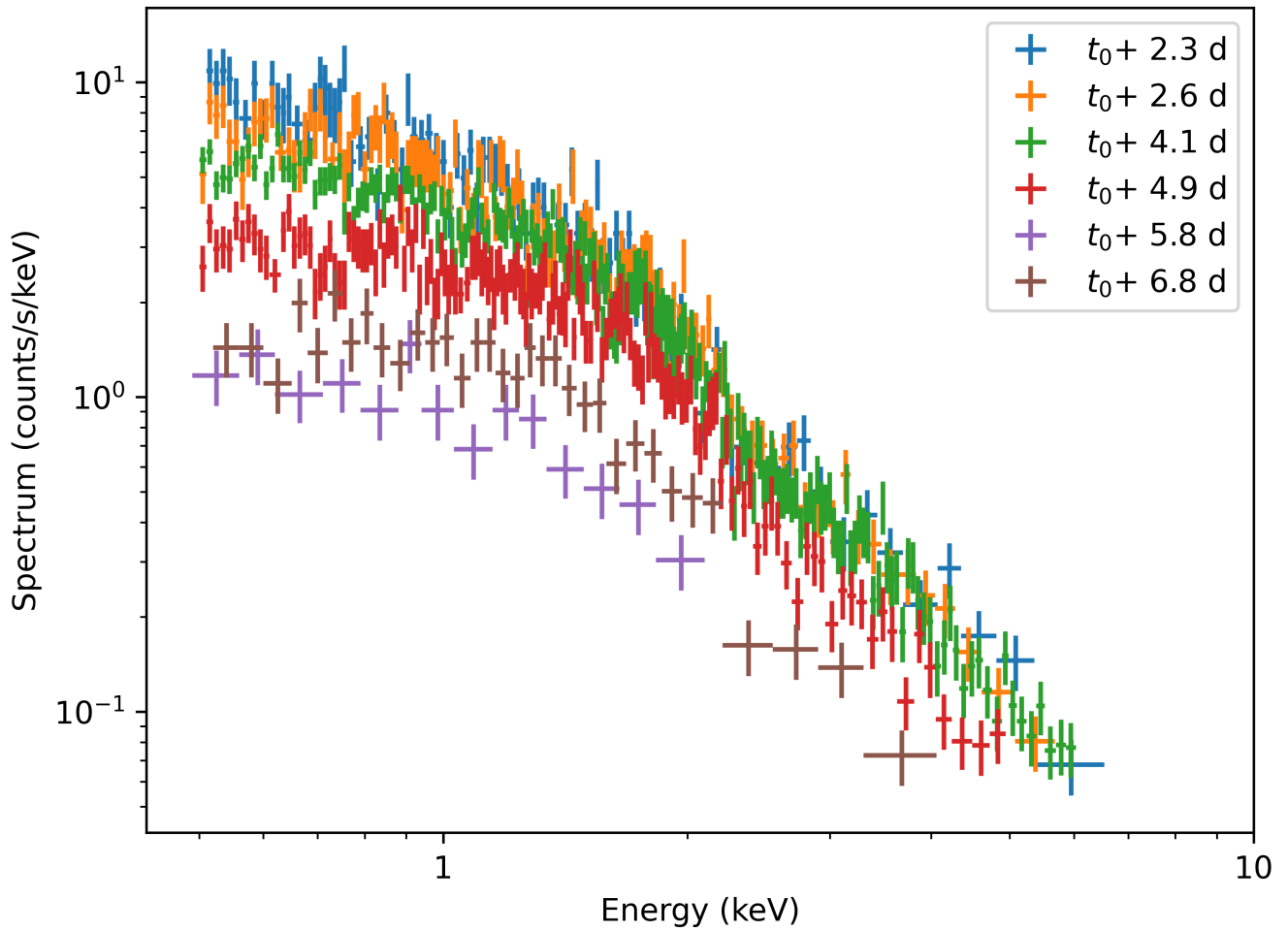


Figure 9 The evolution of the XTI spectra. For clarity, we rebin the spectra to ensure a minimum counts of 25 per bin. For each spectrum, we plot the data up to a critical energy above which the spectrum is dominated by the background. The critical energy varies from observation to observation and lies in the range of ~ 2 – 6 keV.

Table 2 Best-fit parameters of the absorbed power-law model fitted to X-ray spectra.

$t - t_0$ [day]	Inst.	ObsID	Exp. [ks]	N_{H} [10^{21} cm^{-2}]	Γ	$F_{0.5-4 \text{ keV}}$ [10^{-11} cgs]	Cstat/dof	Note
0.0	WXT	155	38.5	1.6*	$1.80^{+0.40}_{-0.37}$	$1.28^{+0.39}_{-0.23}$	145.15/170	
0.0	WXT	155	11.9	1.6*	$2.29^{+1.37}_{-1.09}$	$0.74^{+0.67}_{-0.24}$	78.34/67	pre-flare
0.2	WXT	155	1.2×10^{-2}	1.6*	$0.93^{+1.56}_{-1.49}$	$385.38^{+977.62}_{-176.88}$	0.20/5	flare
0.2	WXT	155	26.6	1.6*	$1.86^{+0.45}_{-0.42}$	$1.29^{+0.49}_{-0.28}$	97.44/134	post-flare
1.6	XRT	001	1.8	1.5 ± 0.4	$2.13^{+0.18}_{-0.17}$	1.20 ± 0.08	25.93/31	
2.0	FXT+XTI	058/101	24.0/0.3	1.6 ± 0.1	2.10 ± 0.03	1.07 ± 0.01	1246.28/1147	joint fit
2.6	XTI	102	0.5	1.6*	$2.09^{+0.06}_{-0.05}$	1.11 ± 0.04	356.23/334	
3.9	XTI	103	2.0	1.6*	$2.00^{+0.04}_{-0.03}$	0.89 ± 0.02	703.17/565	
4.5	XTI	104	1.4	1.6*	$1.94^{+0.04}_{-0.05}$	0.57 ± 0.02	558.78/460	
5.7	XTI	105	0.3	1.6*	$2.52^{+0.27}_{-0.25}$	0.12 ± 0.02	134.97/127	
6.8	XTI	106	0.5	1.6*	2.02 ± 0.14	0.25 ± 0.02	203.09/203	

Notes. columns from left to right: the start time of the observation with respect to $t_0=2024-04-08\text{UT}12:14:12$, in day; the instrument; the observation ID; the exposure time in ks; the neutral hydrogen column density; the photon index; the flux of the 0.5–4 keV band, in $10^{-11} \text{ erg cm}^{-2} \text{ s}^{-1}$; cstat/dof. A superscript asterisk indicates that the parameter is fixed in the spectral fitting. All uncertainties quoted correspond to the 90% confidence level.

ternatively, we use a modified exponential decay model that has the form of $F_X \propto e^{-(t/\tau)^\alpha}$, where F_X is the X-ray flux and t is the time since the first detection in days. This model (dashed gray line) seems to be roughly consistent with the data as well, yielding $F \propto e^{-(t/5.3)^{-5.0}}$, with the critical time $\tau = 5.3$ days, which is close to the transition time determined by the broken power-law fit. Furthermore, the Band function [52], a smoothly broken power-law model, is also employed to fit the flux evolution. However, it does not fit the data adequately, indicating that the transition from the plateau to the steep decay phase is indeed sharp.

The best-fit values of the photon index varied around 2 with time. The evolution of the photon index exhibits a trend that is consistent with the XTI hardness ratio (bottom panel of Fig. 6), as expected. The spectrum hardens during the shallow decay phase, and becomes softer in the observation 7204340101 that was taken ~ 6 days after the trigger. We also present the evolution of the XTI spectrum in Fig. 9, where an apparent hardening of the spectrum with time can be seen in the first 4 observations. The best-fit parameters of the absorbed power-law model are summarised in Table 2.

3.4 Summary of the observed properties

Here we summarize the observed properties of EP240408a:

- EP240408a was initially discovered as an X-ray transient, which was persistent at a flux level of $\sim 10^{-11} \text{ erg cm}^{-2} \text{ s}^{-1}$ in 0.5–4 keV throughout a 83.8 ks-long observation. An intense soft X-ray flare lasting only for ~ 12 s

was also detected, reaching $3.9 \times 10^{-9} \text{ erg cm}^{-2} \text{ s}^{-1}$ or ~ 300 times the persistent X-ray flux. The flare exhibits three peaks, each of a roughly symmetric profile. No other short-timescale variations than the fast flare were found during this observation.

- Further monitoring observations with *EP*, *NICER* and *Swift* reveal that the X-ray emission of EP240408a stayed in a plateau phase that lasts for ~ 4.6 days, followed by a steep decay with time as $\propto t^{-5.5}$. The last significant detection of EP240408a in X-rays was made by *NICER*, approximately 7 days after the trigger. After ~ 10 days, EP240408a became no longer detectable in X-rays. Upper limits can be imposed on its 0.5–4 keV flux as a few times $10^{-13} \text{ erg cm}^{-2} \text{ s}^{-1}$ around 10–20 days and $2 \times 10^{-14} \text{ erg cm}^{-2} \text{ s}^{-1}$ two months after the initial detection. EP240408a was undetected during the WXT observation taken ~ 13 days before the discovery. Hence, the duration of the X-ray emission is found to lie in the range of ~ 7 –23 days, making EP240408a an X-ray transient with an intermediate timescale.

- The X-ray spectrum of EP240408a is non-thermal and can be fit with an absorbed power-law model. The photon index varies with time, ranging from 1.8 to 2.5.

- No counterparts have been found in the optical, NIR and NUV bands, with the earliest observation started 17 hours after the initial X-ray detection and the latest 24 days after, setting upper limits (3σ) to the magnitudes of ~ 21 –22 mag in the various bands.

- No radio emission was detected at ~ 30 days after the

source discovery, with upper limits (5σ upper) of ~ 125 and $\sim 200\mu\text{Jy}$ to the fluxes in the C- and K-bands, respectively.

4 Discussion

Based on its temporal and spectral properties, EP240408a seems to resemble none of the archetypes of the various classes of X-ray transients known so far. The lack of multi-wavelength (in particular optical) counterparts and thus redshift measurement makes it even more difficult to identify its nature. Nevertheless, we try to gain insight into the nature of this peculiar source by comparing its properties with those of the known transient types that are possibly related to EP240408a to some extent, namely TDE with relativistic jets, gamma-ray burst, X-ray binary and fast blue optical transient. We note that, in recent years, there have been findings of fast X-ray transients with timescales of a few kilo-seconds or even shorter, as reported for examples in [18, 19, 53], whose origins are largely unclear although model interpretations have been proposed for some of them. Obviously, the X-ray radiation from EP240408a lasted too long to be possibly associated with any of them.

EP240408a was not detected in the optical or NIR band, even in the very early observations taken within two days after the X-ray trigger. To examine if this is intrinsic or due to strong extinction, we estimate the optical extinction A_V by using the relation between the neutral hydrogen column density N_H and A_V [54], and find $A_V \simeq 0.7$ mag by taking $N_H = 1.6 \times 10^{21} \text{ cm}^{-2}$ as obtained from the X-ray spectral fitting. The value of A_V suggests of merely a factor of two decrease in the V-band flux due to extinction. The extinctions in the longer wavelength J, H, K_s, and r-bands are expected to be even lower, as the extinction monotonically decreases with the wavelength in the optical/NIR band. Therefore, we conclude that EP240408a is intrinsically weak in optical and NIR.

Before proceeding with detailed comparison and discussion, we can constrain the size of the X-ray emitting region from the timescale of the fastest variability, regardless of the physical process of the X-ray emission, as $R_{\text{em}} \lesssim \delta c t_{\text{var}} / (1+z)$, where R_{em} is the characteristic co-moving size of the emitting region, z the redshift, δ the Doppler factor, c the speed of light and t_{var} the observed timescale of the fastest variability. Adopting the timescale of the intense short-term flare of $t_{\text{var}} \sim 12$ s, we can set a limit on the size of the X-ray emitting region (as measured in the co-moving frame of the emitter) in EP240408a as:

$$R_{\text{em}} \lesssim 3.6 \times 10^{11} \frac{\delta}{1+z} \text{ cm}. \quad (1)$$

If EP240408a is powered by a black hole with mass M :

$$R_{\text{em}} \lesssim 1.2 \times 10^6 \frac{\delta}{1+z} \frac{M_{\odot}}{M} R_S, \quad (2)$$

where $R_S \equiv 2GM/c^2$ is the Schwarzschild radius of the black hole with G being the gravitational constant.

4.1 Jetted tidal disruption event

EP240408a has distinct X-ray spectral properties compared to thermal TDEs that are detected in X-ray. Thermal TDEs usually show supersoft thermal X-ray spectra with blackbody temperatures of a few tens of eV (e.g., refs.[8, 55]), especially at the early stage of the outburst. In contrast, EP240408a has a clearly non-thermal spectrum, with a photon index of ~ 2 .

On the other hand, the known jetted TDEs have non-thermal, hard X-ray spectrum, similar to that of EP240408a. The radiation of jetted TDEs is believed to originate from a collimated relativistic jet formed after the tidal disruption process. We compare EP240408a with Sw J1644+57, the prototype jetted TDE and the one with the most extensive dataset among all jetted TDEs known so far. We find the two sharing the following similarities: i) the evolution of the X-rays from Sw J1644+57 also exhibits a plateau phase that lasted for ~ 10 days, followed by a power-law decay [56]. An additional feature in the X-ray light curve of Sw J1644+57 is the extreme flaring activity that is present in the early plateau phase, possibly due to precession or wobbling of the relativistic jet [56]. The short-term flare found in EP240408a may also be explained in the same way, and its much shorter duration than that of Sw J1644+57 may be ascribed to that the bulk of the flare emission is below the moderate sensitivity of EP/WXT. ii) For Sw J1644+57, no transient optical emission was found in the early observations, suggestive of intrinsically weak optical emission produced (e.g., refs.[57, 58]). The optical property of EP240408a is consistent with this picture.

In Fig. 10, we compare the X-ray light curves between EP240408a and three jetted TDEs currently known, namely, Sw J1644+57 (blue), AT2022cmc [59] (orange) and Sw J1112-82 [60] (red). In the plateau phase, Sw J1644+57 is around one order of magnitude brighter than EP240408a. A similar luminosity of the two at the plateau phase would therefore require the host galaxy of EP240408a to be located at a higher redshift of ~ 0.9 than that of Sw J1644+57 (0.35). We also compare the broadband spectral energy distribution (SED) between EP240408a and AT2022cmc in Fig. 11.

If the X-ray flare originated from a relativistic jet aligned close to the line of sight, the Doppler factor $\delta \sim \gamma$, where γ is the Lorentz factor of the jet. The Lorentz factor of jetted TDEs is constrained to be in the range of ~ 10 – 100 [57, 61].

Using equation 1 and assuming $z = 0.9$, we can place an upper limit on the size of the emitting region, as measured in the *host* frame, as $R'_{\text{em}} \lesssim 1.9 \times 10^{13} - 1.9 \times 10^{17}$ cm (here we make use of the fact that the sizes of the emitting region measured in the co-moving and host frames are different by a factor of γ .) The constraint on the emitting size here is consistent with that of Sw J1644+57 [$R'_{\text{em}} \sim 2.3 \times 10^{14} (\gamma/10)^2$ cm; [57]] and AT2022cmc [$R'_{\text{em}} \lesssim 1.2 \times 10^{16} (\gamma/30)^2$ cm; [61]].

On the other hand, EP240408a also shows some other properties that are difficult to explain in the jetted TDE scenario. While both EP240408a and Sw J1644+57 follow a power-law decay after the plateau phase, the decay of EP240408a is much steeper than Sw J1644+57, with the latter showing a canonical $\propto t^{-5/3}$ decay that is consistent with TDE theory. Actually, Sw J1644+57 does show a rapid decay ~ 500 days after trigger that was interpreted as the shutting off of the relativistic jet. If the steep decays of the two share the same physical origin, then a question arises as to why the jet in EP240408a turns off much faster than the jet in Sw J1644+57. In the case of AT2022cmc, no plateau is present in the X-ray light curve, which follows simply a power-law decay $\propto t^{-2}$ [61].

The TDE scenario for EP240408a is further challenged by its weak low-frequency radio and IR emissions observed, in contrast to Sw J1644+57 and AT2022cmc, both showing bright radio emission and IR brightening. The low-frequency synchrotron radiation is expected to be produced from relativistic jets. It is known that the radio emission of jetted TDEs peaks at a much later time than X-rays, i.e. 150 – 200 days later in the case of Sw J1644+57 [62]. We estimate the radio flux of EP240408a at ~ 30 days after the trigger by scaling it with the flux of Sw J1644+57 (~ 20 mJy at ~ 20 GHz) [63] using the flux ratio of the X-ray plateaus (one order of magnitude higher in Sw J1644+57 than in EP240408a). The estimated flux at ~ 20 GHz is ~ 2 mJy, which is much higher than the upper limit of ~ 200 μ Jy derived from the ATCA observations. The deficit of strong radiation at the low frequencies in EP240408a can be clearly seen in Fig. 11 compared to AT2022cmc, which shows much brighter emission in the radio and optical/NIR bands. The weak optical/NIR emission in EP240408a cannot be explained by extinction, given the relatively small value of $A_V \approx 0.7$ mag along its line of sight.

These two issues with the jetted TDE interpretation may be mitigated if the TDE was produced by an intermediate-mass black hole (IMBH). First, the debris fallback timescale $t_{\text{fb}} \approx 4 M_4^{1/2} r_*^{3/2} m_*^{-1}$ days, is much shorter for a lower mass BH than for a higher mass one. This could be in line with the observed early onset of the rapid X-ray decay, if the jet luminosity evolution is tied to that of the debris mass fallback rate. Secondly, one of the most preferable sites that harbors an IMBH is the core of a globular star cluster (e.g., refs [64]),

which are known to lack circum-centre medium. This may explain the non-detection of radio emission at an early time $t \sim 30$ day in EP240408a, since the jet has not yet shock-swept sufficient medium to produce bright synchrotron emission. However, this jetted IMBH-TDE interpretation remains speculative due to the scarcity of the multi-wavelength data.

4.2 Gamma-ray burst

The bright, short-term flare with a duration of 12.3 s is reminiscent of the prompt emission of long gamma-ray bursts. However, the GRB interpretation is challenged by the detection of the relatively stable persistent X-ray emission before and after the flare. Although emission before the main prompt emission, known as precursors, have been observed in both long and short GRBs, the precursor emission is usually a few seconds long with a separation of a few to tens of seconds [68–70], which is clearly different from the persistent, steady emission detected in EP240408a. GRB X-ray afterglow light curves typically have a plateau extending to $10^3 - 10^4$ seconds followed by a decay with a slope of $\sim t^{-1}$ [71]. This is also very different from the observed behavior: the duration of the plateau is much longer and the slope of the post-plateau phase much steeper. EP240408a and GRBs are distinct in their SED as well; for instance, strong radio and optical emission is observed in the afterglow of GRB130427A, as shown in Fig. 11. We therefore conclude that the source is very unlikely to be a GRB.

We note that, EP240315a, a GRB that was also detected by *EP*, exhibits a few interesting features in the soft X-ray band. Its prompt emission in the soft X-ray band (0.5–4 keV) has a significantly longer duration than the prompt emission in the γ -ray band, with a T_{90} of $\sim 1,000$ s in the 0.5–4 keV band compared with a T_{90} of ~ 40 s in the γ -ray band [72]. The trigger in the soft X-ray band is earlier than that in the γ -ray band. Compared with EP240315a, the duration of the steady soft X-ray emission before the short flare is much longer ($\gtrsim 20$ ks). The behaviors of EP240315a in terms of the transition time from the plateau to the power-law decay and the index of the power-law are similar with most GRBs [72] and are therefore different with EP240408a.

4.3 X-ray binary

Another possible scenario is that EP240408a may be an X-ray binary (XRB). XRBs are bright X-ray emitters. In this case, the short-term flare may be a type-I thermonuclear burst that is often seen in neutron star X-ray binaries (NSXRBs). The duration of the normal type-I bursts (in contrast to the intermediate duration bursts or superbursts, both of which are more energetic and have longer durations) is in the range of

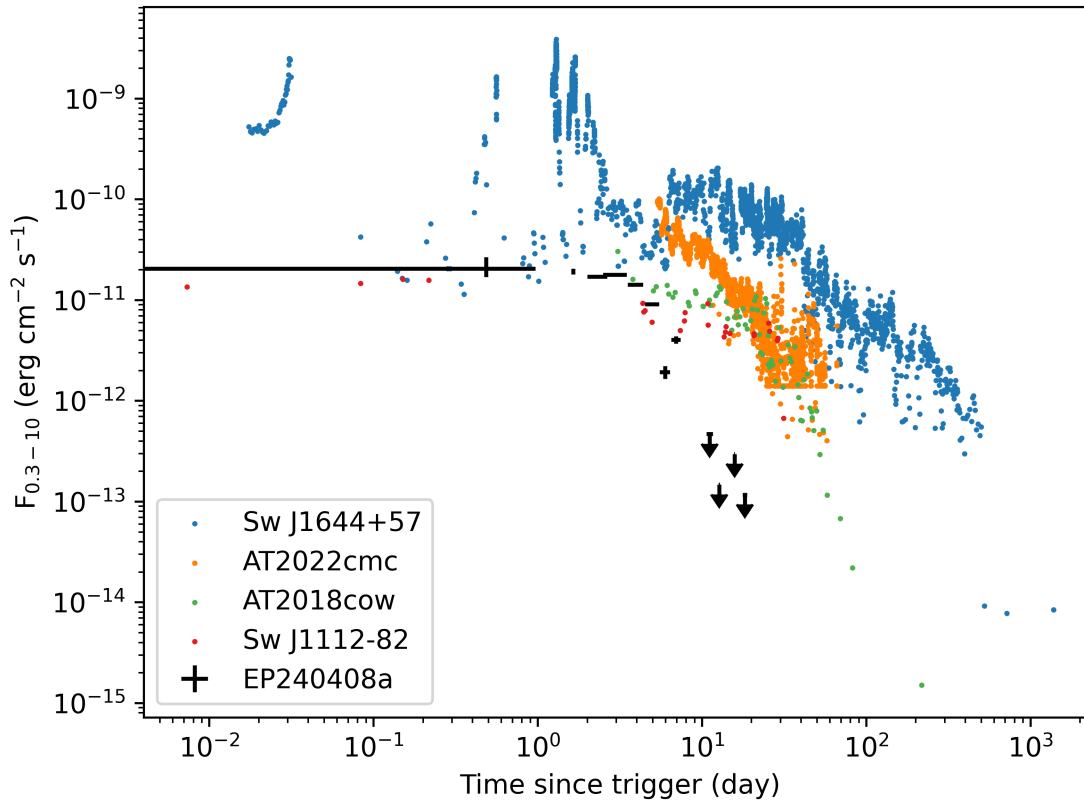


Figure 10 Comparison of EP240408a with Sw J1644+57 (the prototype jetted TDE; blue dots), AT2022cmc (a jetted TDE; orange dots), Sw J1112-82 (a jetted TDE; red dots), and AT2018cow (an FBOT; orange dots) on their long-term X-ray light curves. The light curves of Sw J1644+57 and AT2022cmc are taken from refs. [65]. The light curve of AT2022cmc consists measurements by *NICER* (taken from refs. [59]) and *Swift*, and for the latter we obtain the light curve using the *Swift* online product generator and convert the count rate to flux utilizing WebPIMMS by assuming an X-ray spectra model that is obtained from refs. [61]. The XRT count rate of Sw J1112-82 are also taken from the *Swift* online product generator and converted to 0.3–10 keV flux using WebPIMMS assuming the X-ray spectrum obtained from refs. [60]. For EP240408a, we extrapolate its X-ray flux from the 0.5–4 keV band to the 0.3–10 keV band, assuming the absorbed power-law model with $\Gamma = 2$ and $N_{\text{H}} = 1.6 \times 10^{21} \text{ cm}^{-2}$.

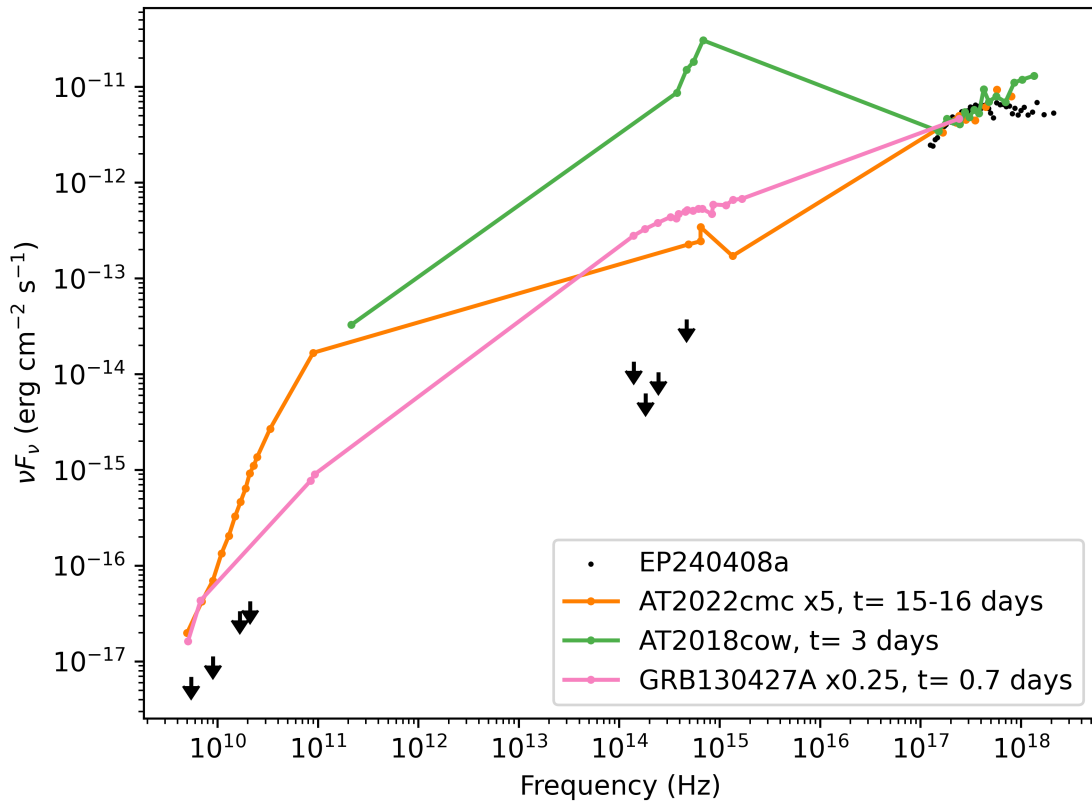


Figure 11 Comparison of EP240408a (black) with AT2022cmc (a jetted TDE; orange), AT2018cow (an FBOT; orange), and GRB130427A (a GRB; pink) on their broadband SED. Data sources: AT2022cmc [59]; AT2018cow [66]; GRB130427A [67]. For AT2022cmc and GRB130427A, the SED is shifted to match EP240408a in the soft X-ray band, as indicated in the plot. The data of EP240408a consist of measurements made with ATCA, GROND, GSP, and FXT-A, and the observations in different energy bands are not simultaneous. For each object other than EP240408a, there are multiple epochs during which quasi-simultaneous radio, optical/IR, and soft X-ray measurements are available, and for constructing the SED we choose the earliest epoch.

10–100 s (e.g., refs. [73]), consistent with the short-term flare seen in EP240408a. Assuming that the flare had reached the Eddington luminosity of a neutron star, the distance to the source would be ~ 18 kpc, leading to the X-ray luminosity of EP240408a during the plateau phase to be a few times 10^{35} erg s^{-1} . However, the profile of the flare is distinct from those of the type-I bursts that typically exhibit a fast rise and an exponential decay. Though the possibility of being an XRB cannot be ruled out, several observed properties of EP240408a seem to be different from those of typical XRBs. EP240408a decays rapidly after the plateau phase within a few days, while the outbursts of XRBs take longer time to decay. Also, XRBs are known to be multi-wavelength emitters, and the intrinsic weakness of EP240408a in the radio, IR, and optical bands would be puzzling if it is an XRB.

4.4 Fast blue optical transient

We also compare EP240408a with the fast blue optical transient (FBOT) AT2018cow [74]. The shapes of the X-ray light curves are quite similar, both with a plateau transitioning to a steep decay. The transition timescale (from plateau to steep decay) of AT2018cow is a bit longer than EP240408a. While the X-ray fluxes of the two during the plateau phase are similar (both at $\sim 10^{-11}$ erg cm^{-2} s^{-1}), they are drastically different in the optical brightness. AT2018cow has a peak brightness of 13.8 mag in the g' -band [74], at least 6 magnitudes brighter than EP240408a, as evidenced in Fig. 11 where a comparison of their SEDs is shown. The sharp contrast makes the FBOT scenario for EP240408a unlikely.

5 Summary

We report the discovery of a new X-ray transient, EP240408a, by *EP*/WXT on April 8th, 2024 and follow-up characterization of the source properties by observations made with space- (*NICER*, *Swift* and *EP*) and ground-based telescopes (including *GROND*, *ATCA*, *NOT*) at multi-wavelengths. Remarkably, a short (lasting for ~ 12 s) yet intense flare occurred once in its X-ray light curve during the 83.8 ks-long WXT observation in which the transient was first detected. The flare reached a flux of 3.9×10^{-9} erg cm^{-2} s^{-1} , ~ 300 times brighter than the persistent flux level of $\sim 10^{-11}$ erg cm^{-2} cm^{-1} in the 0.5–4 keV band.

All the X-ray spectra can be well fitted with an absorbed power-law model, with the photon index varying with time and falling in a range of ~ 1.8 – 2.5 . The X-ray flux appeared to be relatively stable in a plateau phase lasting for 5 days after the trigger, and thereafter decayed rapidly to levels of being undetectable ~ 10 days after the initial detection (5σ upper

limits of a few times 10^{-13} erg cm^{-2} s^{-1}). The characteristic duration of the transient X-ray emission is estimated to lie in between 7–23 days. This makes EP240408a an X-ray transient with an intermediate timescale, in contrast to fast transients (with timescales less than a day or so) and long-term transients (from months to years) that are more commonly found.

No counterparts in the optical, NUV and NIR bands have been found, with limits of around ~ 20 mag set in various optical/NIR bands starting from within one day after the initial X-ray detection. Given the low optical extinction of $A_V \simeq 0.7$ mag, the weakness of the emission in the optical/NIR bands is suggested to be intrinsic. No radio counterparts have been found either based on the ATCA C- and K-band observations performed ~ 30 days after the first X-ray detection.

The observed properties and possible origin of EP240408a are discussed. While EP240408a shares some of the behaviors similar, to some extent, to several well-known types of X-ray transients known so far, including jetted-TDEs, GRBs, FBOTs, and XRBs, we demonstrate that its unique temporal and spectral properties cannot be readily explained by any of these types. Thus, its nature remains an enigma. We suggest that EP240408a may represent a new type of transients with intermediate timescales of the order of ~ 10 days, that may have been missed in previous time-domain X-ray surveys. Any constraints on the redshift of EP240408a would be valuable, which is challenging to measure due to the faintness of its presumed optical counterpart.

EP240408a was discovered two months after *EP*-WXT in operation. Since then no other similar sources have been found in the following six months so far. The *EP* detection rate for similar sources is estimated to be likely 1–2 events per year. Given the X-ray flux levels and timescale of EP240408a, it would be difficult to detect similar objects by other X-ray telescopes or telescopes in other wavebands currently operating. Therefore, it is not surprising that this kind of transients was first discovered by *EP*. Therefore, this discovery is likely to reveal the existence of a potentially new population of transients. *EP* and other future X-ray monitoring missions are expected to detect more of such transients promptly. Meanwhile, timely and deep follow-up observations at multi-wavelengths and measurements of the redshifts of future events are essential for further characterizing their properties and to understand their physical origins.

The authors acknowledge the referee for his/her prompt and valuable comments. This work is based on data obtained with Einstein Probe, a space mission supported by Strategic Priority Program on Space Science of Chinese Academy of Sciences, in collaboration with ESA, MPE and CNES (Grant No. XDA15310000), the Strategic Priority Research Program of the Chinese Academy of Sciences (Grant No. XDB0550200), and the National Key

R&D Program of China (2022YFF0711500). This work is also based on data obtained by the Neil Gehrels Swift Observatory (a NASA/UK/ASI mission) supplied by the UK Swift Science Data Centre at the University of Leicester, as well as on data obtained with NICER, a 0.2–12 keV X-ray telescope operating on the International Space Station, funded by NASA. The Australia Telescope Compact Array is part of the Australia Telescope National Facility (<https://ror.org/05qajvd42>) which is funded by the Australian Government for operation as a National Facility managed by CSIRO. We acknowledge the support by the National Natural Science Foundation of China (Grant Nos. 12333004, 12321003, 12103065, 12373040, 12021003, 12025303, 12393814, 12203071), the China Manned Space Project (Grant Nos. CMS-CSST-2021-A13, CMS-CSST-2021-B11), and the Youth Innovation Promotion Association of the Chinese Academy of Sciences. F.C.Z is supported by a Ramón y Cajal fellowship (grant agreement RYC2021-030888-I). L.G. acknowledges financial support from AGAUR, CSIC, MCIN and AEI 10.13039/501100011033 under projects PID2023-151307NB-I00, PIE 20215AT016, CEX2020-001058-M, and 2021-SGR-01270. We acknowledge the data resources and technical support provided by the China National Astronomical Data Center, the Astronomical Science Data Center of the Chinese Academy of Sciences, and the Chinese Virtual Observatory. Part of the funding for GROND (both hardware and personnel) was generously granted from the Leibniz-Prize to G. Hasinger (DFG grant HA 1850/28-1) and by the Thüringer Landesstern-warte Tautenburg.

Conflict of interest The authors declare that they have no conflict of interest.

- 1 R. A. Remillard and J. E. McClintock, *Annu. Rev. Astron. Astrophys.* **44**, 49 (2006).
- 2 M. J. Rees, *Nature* **333**, 523 (1988).
- 3 N. Bade, S. Komossa, and M. Dahlem, *Astron. Astrophys.* **309**, L35 (1996).
- 4 S. Komossa and J. Greiner, *Astron. Astrophys.* **349**, L45 (1999).
- 5 S. Komossa and N. Bade, *Astron. Astrophys.* **343**, 775 (1999).
- 6 S. Komossa, J. Halpern, N. Schartel, G. Hasinger, M. Santos-Lleo, and P. Predehl, *Astrophys. J. Lett.* **603**, L17 (2004).
- 7 S. Komossa, *J. High Energy Astrophys.* **7**, 148 (2015).
- 8 R. Saxton, S. Komossa, K. Auchettl, and P. G. Jonker, *Space Sci. Rev.* **216**, 85 (2020).
- 9 J. P. Pye and I. M. McHardy, *Mon. Not. R. Astron. Soc.*, **205**, 875 (1983).
- 10 V. A. Arefiev, W. C. Priedhorsky, and K. N. Borozdin, *Astrophys. J.* **586**, 1238 (2003).
- 11 B. Zhang, *The Physics of Gamma-Ray Bursts*, (Cambridge Univ. Press, Cambridge, 2018).
- 12 J. Heise, J. I. Zand, R. M. Kippen, and P. M. Woods, in *Gamma-Ray Bursts in the Afterglow Era*, (edited by E. Costa, F. Frontera, and J. Hjorth), 16, (Springer-Verlag, 2001).
- 13 N. Rea and P. Esposito, in *High-Energy Emission from Pulsars and Their Systems*, 247, (Springer-Verlag, Berlin Heidelberg, 2011), arXiv: 1101.4472
- 14 R. Turolla, S. Zane, and A. L. Watts, *Rep. Prog. Phys.* **78**, 116901 (2015).
- 15 A. M. Soderberg, E. Berger, K. L. Page, P. Schady, J. Parrent, D. Pooley, X. Y. Wang, E. O. Ofek, A. Cucchiara, A. Rau, E. Waxman, J. D. Simon, D. C. J. Bock, P. A. Milne, M. J. Page, J. C. Barentine, S. D. Barthelmy, A. P. Beardmore, M. F. Bietenholz, P. Brown, A. Burrows, D. N. Burrows, G. Byrgelson, S. B. Cenko, P. Chandra, J. R. Cummings, D. B. Fox, A. Gal-Yam, N. Gehrels, S. Immler, M. Kasliwal, A. K. H. Kong, H. A. Krimm, S. R. Kulkarni, T. J. Maccarone, P. Mészáros, E. Nakar, P. T. O'Brien, R. A. Overzier, M. de Pasquale, J. Racusin, N. Rea, and D. G. York, *Nature* **453**, 469 (2008).
- 16 D. Alp and J. Larsson, *Astrophys. J.* **896**, 39 (2020).
- 17 A. O. Benz and M. Güdel, *Annu. Rev. Astron. Astrophys.* **48**, 241 (2010).
- 18 F. E. Bauer, E. Treister, K. Schawinski, S. Schulze, B. Luo, D. M. Alexander, W. N. Brandt, A. Comastri, F. Forster, R. Gilli, D. A. Kann, K. Maeda, K. Nomoto, M. Paolillo, P. Ranalli, D. P. Schneider, O. Shemmer, M. Tanaka, A. Tolstov, N. Tominaga, P. Tozzi, C. Vignali, J. Wang, Y. Xue, and G. Yang, *Mon. Not. R. Astron. Soc.* **467**, 4841 (2017).
- 19 Y. Q. Xue, X. C. Zheng, Y. Li, W. N. Brandt, B. Zhang, B. Luo, B.-B. Zhang, F. E. Bauer, H. Sun, B. D. Lehmer, X.-F. Wu, G. Yang, X. Kong, J. Y. Li, M. Y. Sun, J.-X. Wang, and F. Vito, *Nature* **568**, 198 (2019).
- 20 J. Quirola-Vásquez, F. E. Bauer, P. G. Jonker, W. N. Brandt, G. Yang, A. J. Levan, Y. Q. Xue, D. Eappachen, X. C. Zheng, and B. Luo, *Astron. Astrophys.* **663**, A168 (2022).
- 21 J. Quirola-Vásquez, F. E. Bauer, P. G. Jonker, W. N. Brandt, G. Yang, A. J. Levan, Y. Q. Xue, D. Eappachen, E. Camacho, M. E. Ravasio, X. C. Zheng, and B. Luo, *Astron. Astrophys.* **675**, A44 (2023).
- 22 A. Marino, H. Yang, F. Coti Zelati, N. Rea, S. Guillot, G. K. Jaisawal, C. Maitra, F. Haberl, E. Kuulkers, W. Yuan, H. Feng, L. Tao, C. Jin, H. Sun, W. Zhang, W. Chen, E. P. J. van den Heuvel, R. Soria, B. Zhang, S. S. Weng, L. Ji, G. B. Zhang, X. Pan, Z. Lv, C. Zhang, Z. Ling, Y. Chen, S. Jia, Y. Liu, J. U. Ness, H. Q. Cheng, D. Y. Li, K. C. Gendreau, M. Ng, and T. E. Strohmayer, (2024), arXiv: 2407.21371
- 23 W. Yuan, C. Zhang, Y. Chen, and Z. Ling, in *Handbook of X-ray and Gamma-ray Astrophysics*, (edited by C. Bambi and A. Santangelo), 86, (Springer Singapore, 2022).
- 24 Y. Chen, W. Cui, D. Han, J. Wang, Y. Yang, Y. Wang, W. Li, J. Ma, Y. Xu, F. Lu, H. Chen, Q. Tang, W. Yuan, P. Friedrich, N. Meidinger, I. Keil, V. Burwitz, J. Eder, K. Hartmann, K. Nandra, A. Keereman, A. Santovincenzo, D. Vernani, G. Bianucci, G. Valsecchi, B. Wang, L. Wang, D. Wang, D. Li, L. Sheng, P. Qiang, R. Shi, X. Chao, Z. Song, Z. Zhang, J. Huo, H. Wang, M. Cong, X. Yang, D. Hou, X. Zhao, Z. Zhao, T. Chen, M. Li, T. Zhang, L. Luo, J. Xu, G. Li, Q. Zhang, X. Bi, Y. Zhu, N. Yu, C. Chen, Z. Lv, B. Lu, and J. Zhang, *SPIE* **11444**, 114445B (2020).
- 25 J. W. Hu, D. H. Zhao, Y. Liu, Z. X. Ling, C. Zhang, C. C. Jin, H. Q. Cheng, W. Chen, C. Z. Cui, D. W. Fan, H. B. Hu, M. H. Huang, D. Y. Li, T. Y. Lian, H. Y. Liu, M. J. Liu, Z. Z. Lv, X. Mao, H. W. Pan, X. Pan, H. Sun, W. X. Wang, Y. L. Wang, Q. Y. Wu, X. P. Xu, Y. F. Xu, H. N. Yang, W. Yuan, M. Zhang, W. D. Zhang, W. J. Zhang, Z. Zhang, E. Kuulkers, A. Santovincenzo, P. O'Brien, K. Nandra, A. Rau, B. Cordier, and Einstein Probe Team, *GRB Coordinates Network* **36053**, 1 (2024).
- 26 N. Gehrels, G. Chincarini, P. Giommi, K. O. Mason, J. A. Nousek, A. A. Wells, N. E. White, S. D. Barthelmy, D. N. Burrows, L. R. Cominsky, K. C. Hurley, F. E. Marshall, P. Mészáros, P. W. A. Roming, L. Angelini, L. M. Barbier, T. Belloni, S. Campana, P. A. Caraveo, M. M. Chester, O. Citterio, T. L. Cline, M. S. Cropper, J. R. Cummings, A. J. Dean, E. D. Feigelson, E. E. Fenimore, D. A. Frail, A. S. Fruchter, G. P. Garmire, K. Gendreau, G. Ghisellini, J. Greiner, J. E. Hill, S. D. Hunsberger, H. A. Krimm, S. R. Kulkarni, P. Kumar, F. Lebrun, N. M. Lloyd-Ronning, C. B. Markwardt, B. J. Mattson, R. F. Mushotzky, J. P. Norris, J. Osborne, B. Paczynski, D. M. Palmer, H. S. Park, A. M. Parsons, J. Paul, M. J. Rees, C. S. Reynolds, J. E. Rhoads, T. P. Sasseen, B. E. Schaefer, A. T. Short, A. P. Smale, I. A. Smith, L. Stella, G. Tagliferri, T. Takahashi, M. Tashiro, L. K. Townsley, J. Tueller, M. J. L. Turner, M. Vietri, W. Voges, M. J. Ward, R. Willingale, F. M. Zerbi, and W. Zhang, *Astrophys. J.* **611**, 1005 (2004).
- 27 J. W. Hu, D. H. Zhao, Y. Liu, Z. X. Ling, C. Zhang, C. C. Jin, H. Q. Cheng, W. Chen, C. Z. Cui, D. W. Fan, H. B. Hu, M. H. Huang, D. Y. Li, T. Y. Lian, H. Y. Liu, M. J. Liu, Z. Z. Lv, X. Mao, H. W. Pan, X. Pan, H. Sun, W. X. Wang, Y. L. Wang, Q. Y. Wu, X. P. Xu, Y. F. Xu, H. N. Yang, W. Yuan, M. Zhang, W. D. Zhang, W. J. Zhang, Z. Zhang, E. Kuulkers, A. Santovincenzo, P. O'Brien, K. Nandra, A. Rau, B. Cordier, and Einstein Probe Team, *GRB Coordinates Network* **36057**, 1 (2024).
- 28 N. Rea, F. Coti Zelati, A. Marino, E. Kuulkers, Y. Chen, S. M. Jia, C. K. Li, W. W. Cui, H. Feng, J. Guan, D. W. Han, W. Li, C. Z. Liu, F. J. Lu, L. M. Song, L. Tao, J. Wang, J. J. Xu, J. Zhang, S. N. Zhang, H. S.

- Zhao, X. F. Zhao, J. W. Hu, C. C. Jin, D. Y. Li, Z. X. Ling, H. Y. Liu, Y. Liu, H. Sun, W. Yuan, C. Zhang, D. H. Zhao, P. G. Jonker, A. Santovincenzo, P. O'Brien, K. Nandra, A. Rau, P. Friedrich, N. Meidinger, V. Burwitz, and B. Cordi, *The Astronomer's Telegram* **16584**, 1 (2024).
- 29 D. N. Burrows, J. E. Hill, J. A. Nousek, J. A. Kennea, A. Wells, J. P. Osborne, A. F. Abbey, A. Beardmore, K. Mukerjee, A. D. T. Short, G. Chincarini, S. Campana, O. Citterio, A. Moretti, C. Pagani, G. Tagliaferri, P. Giommi, M. Capalbi, F. Tamburelli, L. Angelini, G. Cusumano, H. W. Bräuninger, W. Burkert, and G. D. Hartner, *Space Sci. Rev.* **120**, 165 (2005).
- 30 P. W. A. Roming, T. E. Kennedy, K. O. Mason, J. A. Nousek, L. Ahr, R. E. Bingham, P. S. Broos, M. J. Carter, B. K. Hancock, H. E. Huckle, S. D. Hunsberger, H. Kawakami, R. Killough, T. S. Koch, M. K. McLelland, K. Smith, P. J. Smith, J. C. Soto, P. T. Boyd, A. A. Breeveld, S. T. Holland, M. Ivanushkina, M. S. Pryzby, M. D. Still, and J. Stock, *Space Sci. Rev.* **120**, 95 (2005).
- 31 K. C. Gendreau, Z. Arzoumanian, P. W. Adkins, C. L. Albert, J. F. Anders, A. T. Aylward, C. L. Baker, E. R. Balsamo, W. A. Bamford, S. S. Benegalrao, D. L. Berry, S. Bhalwani, J. K. Black, C. Blaurock, G. M. Bronke, G. L. Brown, J. G. Budinoff, J. D. Cantwell, T. Cazeau, P. T. Chen, T. G. Clement, A. T. Colangelo, J. S. Coleman, J. D. Cooper-Smith, W. E. Dehaven, J. P. Doty, M. D. Egan, T. Enoto, T. W. Fan, D. M. Ferro, R. Foster, N. M. Galassi, L. D. Gallo, C. M. Green, D. Grosh, K. Q. Ha, M. A. Hasounch, K. B. Heefner, P. Hestnes, L. J. Hoge, T. M. Jacobs, J. L. Jørgensen, M. A. Kaiser, J. W. Kellogg, S. J. Kenyon, R. G. Koenecke, R. P. Kozon, B. LaMarr, M. D. Lambertson, A. M. Larson, S. Lentine, J. H. Lewis, M. G. Lilly, K. A. Liu, A. Malonis, S. S. Manthripragada, C. B. Markwardt, B. D. Matonak, I. E. McGinnis, R. L. Miller, A. L. Mitchell, J. W. Mitchell, J. S. Mohammed, C. A. Monroe, K. M. Mont de Garcia, P. D. Mulé, L. T. Nagao, S. N. Ngo, E. D. Norris, D. A. Norwood, J. Novotka, T. Okajima, L. G. Olsen, C. O. Onyeachu, H. Y. Orosco, J. R. Peterson, K. N. Pevear, K. K. Pham, S. E. Pollard, J. S. Pope, D. F. Powers, C. E. Powers, S. R. Price, G. Y. Prigozhin, J. B. Ramirez, W. J. Reid, R. A. Remillard, E. M. Rogstad, G. P. Rosecrans, J. N. Rowe, J. A. Sager, C. A. Sanders, B. Savadkin, M. R. Saylor, A. F. Schaeffer, N. S. Schweiss, S. R. Semper, P. J. Serlemitsos, L. V. Shackelford, Y. Soong, J. Strubel, M. L. Vezie, J. S. Villasenor, L. B. Winternitz, G. I. Wofford, M. R. Wright, M. Y. Yang, and W. H. Yu, *SPIE* **9905**, 99051H (2016).
- 32 P. A. Evans, A. P. Beardmore, K. L. Page, J. P. Osborne, P. T. O'Brien, R. Willingale, R. L. C. Starling, D. N. Burrows, O. Godet, L. Vetere, J. Racusin, M. R. Goad, K. Wiersema, L. Angelini, M. Capalbi, G. Chincarini, N. Gehrels, J. A. Kennea, R. Margutti, D. C. Morris, C. J. Mountford, C. Pagani, M. Perri, P. Romano, and N. Tanvir, *Mon. Not. R. Astron. Soc.* **397**, 1177 (2009).
- 33 P. Predehl, R. Andritschke, V. Arefiev, V. Babyshkin, O. Batanov, W. Becker, H. Böhringer, A. Bogomolov, T. Boller, K. Borm, W. Bornemann, H. Bräuninger, M. Brüggen, H. Brunner, M. Brusa, E. Bulbul, M. Buntov, V. Burwitz, W. Burkert, N. Clerc, E. Churazov, D. Coutinho, T. Dauser, K. Dennerl, V. Doroshenko, J. Eder, V. Emberger, T. Eraerds, A. Finoguenov, M. Freyberg, P. Friedrich, S. Friedrich, M. Fürmetz, A. Georgakakis, M. Gilfanov, S. Granato, C. Grossberger, A. Gueguen, P. Gureev, F. Haberl, O. Hälker, G. Hartner, G. Hasinger, H. Huber, L. Ji, A. v. Kienlin, W. Kink, F. Korotkov, I. Kreykenbohm, G. Lamer, I. Lomakin, I. Lapshov, T. Liu, C. Maitra, N. Meidinger, B. Menz, A. Merloni, T. Mernik, B. Mican, J. Mohr, S. Müller, K. Nandra, V. Nazarov, F. Pacaud, M. Pavlinsky, E. Perinati, E. Pfeffermann, D. Pietschner, M. E. Ramos-Ceja, A. Rau, J. Reiffers, T. H. Reiprich, J. Robrade, M. Salvato, J. Sanders, A. Santangelo, M. Sasaki, H. Scheuerle, C. Schmid, J. Schmitt, A. Schwöpe, A. Shirshakov, M. Steinmetz, I. Stewart, L. Strüder, R. Sunyaev, C. Tenzer, L. Tiedemann, J. Trümper, V. Voron, P. Weber, J. Wilms, and V. Yaroshenko, *Astron. Astrophys.* **647**, A1 (2021).
- 34 A. Merloni, G. Lamer, T. Liu, M. E. Ramos-Ceja, H. Brunner, E. Bulbul, K. Dennerl, V. Doroshenko, M. J. Freyberg, S. Friedrich, E. Gatuazz, A. Georgakakis, F. Haberl, Z. Igo, I. Kreykenbohm, A. Liu, C. Maitra, A. Malyali, M. G. F. Mayer, K. Nandra, P. Predehl, J. Robrade, M. Salvato, J. S. Sanders, I. Stewart, D. Tubín-Arenas, P. Weber, J. Wilms, R. Arcodia, E. Artis, J. Aschersleben, A. Avakyan, C. Aydar, Y. E. Bahar, F. Balzer, W. Becker, K. Berger, T. Boller, W. Bornemann, M. Brüggen, M. Brusa, J. Buchner, V. Burwitz, F. Camilloni, N. Clerc, J. Comparat, D. Coutinho, S. Czesla, S. M. Dannhauer, L. Dauner, T. Dauser, J. Dietl, K. Dolag, T. Dwelly, K. Egg, E. Ehl, S. Freund, P. Friedrich, R. Gaida, C. Garrel, V. Ghirardini, A. Gokus, G. Grünwald, S. Grandis, I. Grotova, D. Gruen, A. Gueguen, S. Hämmerich, N. Hamaus, G. Hasinger, K. Haubner, D. Homan, J. Ider Chitham, W. M. Joseph, A. Joyce, O. König, D. M. Kaltenbrunner, A. Khokhriakova, W. Kink, C. Kirsch, M. Kluge, J. Knies, S. Krippendorf, M. Krumpe, J. Kurpas, P. Li, Z. Liu, N. Locatelli, M. Lorenz, S. Müller, E. Magaudda, C. Mannes, H. McCall, N. Meidinger, M. Michailidis, K. Migkas, D. Muñoz-Giraldo, B. Musimenta, N. T. Nguyen-Dang, Q. Ni, A. Olechowska, N. Ota, F. Pacaud, T. Pasini, E. Perinati, A. M. Pires, C. Pommranz, G. Ponti, K. Poppenhaeger, G. Pühlhofer, A. Rau, M. Reh, T. H. Reiprich, W. Roster, S. Saeedi, A. Santangelo, M. Sasaki, J. Schmitt, P. C. Schneider, T. Schrabback, N. Schuster, A. Schwöpe, R. Seppi, M. M. Serim, S. Shreeram, E. Sokolova-Lapa, H. Starck, B. Stelzer, J. Stierhof, V. Suleimanov, C. Tenzer, I. Traulsen, J. Trümper, K. Tsuge, T. Urrutia, A. Veronica, S. G. H. Waddell, R. Willer, J. Wolf, M. C. H. Yeung, A. Zainab, F. Zangrandi, X. Zhang, Y. Zhang, and X. Zheng, *Astron. Astrophys.* **682**, A34 (2024).
- 35 D. Tubín-Arenas, M. Krumpe, G. Lamer, J. Haase, J. Sanders, H. Brunner, D. Homan, A. Schwöpe, A. Georgakakis, K. Poppenhaeger, I. Traulsen, O. König, A. Merloni, A. Gueguen, A. Strong, and Z. Liu, *Astron. Astrophys.* **682**, A35 (2024).
- 36 Y. Li, X. Wen, X. Sun, X. Liu, X. Liang, D. Guo, W. Peng, K. Gong, G. Li, H. Wang, S. Xiong, J. Liao, H. Lu, J. Wang, Z. An, D. Zhang, M. Gao, G. Chen, Y. Liu, S. Yang, R. Qiao, F. Zhang, X. Zhao, Y. Xu, Y. Zhu, and X. Li, *Sci. China-Phys. Mech. Astron.* **50**, 129508 (2020).
- 37 C.-W. Wang, S.-L. Xiong, J.-C. Liu, C.-K. Li, C. Zheng, and Gecam Team, *GRB Coordinates Network* **36058**, 1 (2024).
- 38 J. Greiner, W. Bornemann, C. Clemens, M. Deuter, G. Hasinger, M. Honsberg, H. Huber, S. Huber, M. Krauss, T. Krühler, A. Küpcü Yoldaş, H. Mayer-Hasselwander, B. Mican, N. Primak, F. Schrey, I. Steiner, G. Szokoly, C. C. Thöne, A. Yoldaş, S. Klose, U. Laux, and J. Winkler, *Publ. Astron. Soc. Pac.* **120**, 405 (2008).
- 39 T. Krühler, A. Küpcü Yoldaş, J. Greiner, C. Clemens, S. McBreen, N. Primak, S. Savaglio, A. Yoldaş, G. P. Szokoly, and S. Klose, *Astrophys. J.* **685**, 376 (2008).
- 40 M. F. Skrutskie, R. M. Cutri, R. Stiening, M. D. Weinberg, S. Schneider, J. M. Carpenter, C. Beichman, R. Capps, T. Chester, J. Elias, J. Huchra, J. Liebert, C. Lonsdale, D. G. Monet, S. Price, P. Seitzer, T. Jarrett, J. D. Kirkpatrick, J. E. Gizis, E. Howard, T. Evans, J. Fowler, L. Fullmer, R. Hurt, R. Light, E. L. Kopan, K. A. Marsh, H. L. McCallon, R. Tam, S. Van Dyk, and S. Wheelock, *Astron. J.* **131**, 1163 (2006).
- 41 A. Rau, *GRB Coordinates Network* **36059**, 1 (2024).
- 42 W. X. Li, S. J. Xue, D. Xu, M. Andrews, J. Farrah, D. A. Howell, M. Newsome, E. Padilla Gonzalez, C. McCully, and G. Terreran, *GRB Coordinates Network* **36079**, 1 (2024).
- 43 G. Antipov, V. Lipunov, P. Balanutsa, D. Buckley, K. Zhirkov, A. Kuznetsov, N. Tiurina, E. Gorboskoy, Ya. Kechin, D. Vlasenko, Yu. Tselik, I. Gorbunov, V. Vladimirov, D. Zimnukhov, V. Senik, A. Yudin, A. Chasovnikov, D. Cheryasov, O. Gress, N. Budnev, A. Sosnovskij, C. Francile, F. Podesta, R. Podesta, R. Rebolo, M. Serra, A. Tlatov, D. Dormidontov, A. Gabovich, and V. Yurkov, *GRB Coordinates Network* **36060**, 1 (2024).
- 44 I. Perez-Garcia, E. Fernandez-Garcia, M. D. Caballero-Garcia, R. Sanchez-Ramirez, S. Guziy, S. Y. Wu, A. J. Castro-Tirado, P. J. Meintjes, H. J. van Heerden, A. Martin-Carrillo, L. Hanlon, M. Gritse-

- vich, and C. J. Perez del Pulgar, *GRB Coordinates Network* **36056**, 1 (2024).
- 45 J. P. McMullin, B. Waters, D. Schiebel, W. Young, and K. Golap, in *Astronomical Data Analysis Software and Systems XVI. Astron. Soc. Pac.* (edited by R. Shaw, A., F. Hill, and D. Bell, J.), volume 376 of *Astronomical Data Analysis Software and Systems XVI ASP Conference Series*, 127, (San Francisco 2007).
- 46 J. D. Scargle, J. P. Norris, B. Jackson, and J. Chiang, *Astrophys. J.* **764**, 167 (2013).
- 47 A. De Luca, R. Salvaterra, A. Belfiore, S. Carpano, D. D'Agostino, F. Haberl, G. L. Israel, D. Law-Green, G. Lisini, M. Marelli, G. Novara, A. M. Read, G. Rodriguez-Castillo, S. R. Rosen, D. Salvetti, A. Tiengo, G. Vianello, M. G. Watson, C. Delvaux, T. Dickens, P. Esposito, J. Greiner, H. Hämmerle, A. Kreikenbohm, S. Kreykenbohm, M. Oertel, D. Pizzocaro, J. P. Pye, S. Sandrelli, B. Stelzer, J. Wilms, and F. Zagaria, *Astron. Astrophys.* **650**, A167 (2021).
- 48 K. A. Arnaud, in *ASP Conf. Ser. 101*, (edited by J. H. Jacoby and J. Barnes), volume 101, 17, (ASP, San Francisco, CA, 1996).
- 49 W. Cash, *Astrophys. J.* **228**, 939 (1979).
- 50 J. Wilms, A. Allen, and R. McCray, *Astrophys. J.* **542**, 914 (2000).
- 51 HI4PI Collaboration, N. Ben Bekhti, L. Flöer, R. Keller, J. Kerp, D. Lenz, B. Winkel, J. Bailin, M. R. Calabretta, L. Dedes, H. A. Ford, B. K. Gibson, U. Haud, S. Janowiecki, P. M. W. Kalberla, F. J. Lockman, N. M. McClure-Griffiths, T. Murphy, H. Nakanishi, D. J. Pisano, and L. Staveley-Smith, *Astron. Astrophys.* **594**, A116 (2016).
- 52 D. Band, J. Matteson, L. Ford, B. Schaefer, D. Palmer, B. Teegarden, T. Cline, M. Briggs, W. Paciesas, G. Pendleton, G. Fishman, C. Kouveliotou, C. Meegan, R. Wilson, and P. Lestrade, *Astrophys. J.* **413**, 281 (1993).
- 53 J. A. Irwin, W. P. Maksym, G. R. Sivakoff, A. J. Romanowsky, D. Lin, T. Speegle, I. Prado, D. Mildebrath, J. Strader, J. Liu, and J. M. Miller, *Nature* **538**, 356 (2016).
- 54 T. Güver and F. Özel, *Mon. Not. R. Astron. Soc.* **400**, 2050 (2009).
- 55 S. Gezari, *Annu. Rev. Astron. Astrophys.* **59** (2021).
- 56 A. Tchekhovskoy, B. D. Metzger, D. Giannios, and L. Z. Kelley, *Mon. Not. R. Astron. Soc.* **437**, 2744 (2014).
- 57 J. S. Bloom, D. Giannios, B. D. Metzger, S. B. Cenko, D. A. Perley, N. R. Butler, N. R. Tanvir, A. J. Levan, P. T. O'Brien, L. E. Strubbe, F. De Colle, E. Ramirez-Ruiz, W. H. Lee, S. Nayakshin, E. Quataert, A. R. King, A. Cucchiara, J. Guillochon, G. C. Bower, A. S. Fruchter, A. N. Morgan, and A. J. van der Horst, *Science* **333**, 203 (2011).
- 58 A. J. Levan, N. R. Tanvir, S. B. Cenko, D. A. Perley, K. Wiersema, J. S. Bloom, A. S. Fruchter, A. d. U. Postigo, P. T. O'Brien, N. Butler, A. J. van der Horst, G. Leloudas, A. N. Morgan, K. Misra, G. C. Bower, J. Farihi, R. L. Tunnicliffe, M. Modjaz, J. M. Silverman, J. Hjorth, C. Thöne, A. Cucchiara, J. M. C. Cerón, A. J. Castro-Tirado, J. A. Arnold, M. Bremer, J. P. Brodie, T. Carroll, M. C. Cooper, P. A. Curran, R. M. Cutri, J. Ehle, D. Forbes, J. Fynbo, J. Gorosabel, J. Graham, D. I. Hoffman, S. Guziy, P. Jakobsson, A. Kamble, T. Kerr, M. M. Kasliwal, C. Kouveliotou, D. Kocevski, N. M. Law, P. E. Nugent, E. O. Ofek, D. Poznanski, R. M. Quimby, E. Rol, A. J. Romanowsky, R. Sánchez-Ramírez, S. Schulze, N. Singh, L. van Spaandonk, R. L. C. Starling, R. G. Strom, J. C. Tello, O. Vaduvescu, P. J. Wheatley, R. A. M. J. Wijers, J. M. Winters, and D. Xu, *Science* **333**, 199 (2011).
- 59 D. R. Pasham, M. Lucchini, T. Laskar, B. P. Gompertz, S. Srivastav, M. Nicholl, S. J. Smartt, J. C. A. Miller-Jones, K. D. Alexander, R. Fender, G. P. Smith, M. Fulton, G. Dewangan, K. Gendreau, E. R. Coughlin, L. Rhodes, A. Horesh, S. van Velzen, I. Sfaradi, M. Guolo, N. Castro Segura, A. Aamer, J. P. Anderson, I. Arcavi, S. J. Brennan, K. Chambers, P. Charalampopoulos, T.-W. Chen, A. Clocchiatti, T. de Boer, M. Dennefeld, E. Ferrara, L. Galbany, H. Gao, J. H. Gillanders, A. Goodwin, M. Gromadzki, M. Huber, P. G. Jonker, M. Joshi, E. Kara, T. L. Killestein, P. Kosec, D. Kocevski, G. Leloudas, C.-C. Lin, R. Margutti, S. Mattila, T. Moore, T. Müller-Bravo, C.-C. Ngeow, S. Oates, F. Onori, Y.-C. Pan, M. Perez-Torres, P. Rani, R. Remillard, E. J. Ridley, S. Schulze, X. Sheng, L. Shingles, K. W. Smith, J. F. Steiner, R. Wainscoat, T. Wevers, and S. Yang, *Nature Astronomy* **7**, 88 (2023).
- 60 G. C. Brown, A. J. Levan, E. R. Stanway, N. R. Tanvir, S. B. Cenko, E. Berger, R. Chornock, and A. Cucchiara, *Mon. Not. R. Astron. Soc.* **452**, 4297 (2015).
- 61 Y. Yao, W. Lu, F. Harrison, S. R. Kulkarni, S. Gezari, M. Guolo, S. B. Cenko, and A. Y. Q. Ho, *Astrophys. J.* **965**, 39 (2024).
- 62 B. A. Zauderer, E. Berger, R. Margutti, G. G. Pooley, R. Sari, A. M. Soderberg, A. Brunthaler, and M. F. Bietenholz, *Astrophys. J.* **767**, 152 (2013).
- 63 B. A. Zauderer, E. Berger, A. M. Soderberg, A. Loeb, R. Narayan, D. A. Frail, G. R. Petitpas, A. Brunthaler, R. Chornock, J. M. Carpenter, G. G. Pooley, K. Mooley, S. R. Kulkarni, R. Margutti, D. B. Fox, E. Nakar, N. A. Patel, N. H. Volgenau, T. L. Culverhouse, M. F. Bietenholz, M. P. Rupen, W. Max-Moerbeck, A. C. S. Readhead, J. Richards, M. Shepherd, S. Storm, and C. L. H. Hull, *Nature* **476**, 425 (2011).
- 64 D. Lin, J. Strader, E. R. Carrasco, D. Page, A. J. Romanowsky, J. Homan, J. A. Irwin, R. A. Remillard, O. Godet, N. A. Webb, H. Baumgardt, R. Wijnands, D. Barret, P.-A. Duc, J. P. Brodie, and S. D. J. Gwyn, *Nature Astronomy* **2**, 656 (2018).
- 65 A. Polzin, R. Margutti, D. L. Coppejans, K. Auchettl, K. L. Page, G. Vasilopoulos, J. S. Bright, P. Esposito, P. K. G. Williams, K. Mukai, and E. Berger, *Astrophys. J.* **959**, 75 (2023).
- 66 R. Margutti, B. D. Metzger, R. Chornock, I. Vurm, N. Roth, B. W. Grefenstette, V. Savchenko, R. Cartier, J. F. Steiner, G. Terreran, B. Margalit, G. Migliori, D. Milisavljevic, K. D. Alexander, M. Bietenholz, P. K. Blanchard, E. Bozzo, D. Brethauer, I. V. Chilingarian, D. L. Coppejans, L. Ducci, C. Ferrigno, W. Fong, D. Götz, C. Guidorzi, A. Hajela, K. Hurley, E. Kuulkers, P. Laurent, S. Mereghetti, M. Nicholl, D. Patnaude, P. Ubertini, J. Banovetz, N. Bartel, E. Berger, E. R. Coughlin, T. Eftekhari, D. D. Frederiks, A. V. Kozlova, T. Laskar, D. S. Svinikin, M. R. Drout, A. MacFadyen, and K. Paterson, *Astrophys. J.* **872**, 18 (2019).
- 67 D. A. Perley, S. B. Cenko, A. Corsi, N. R. Tanvir, A. J. Levan, D. A. Kann, E. Sonbas, K. Wiersema, W. Zheng, X. H. Zhao, J. M. Bai, M. Bremer, A. J. Castro-Tirado, L. Chang, K. I. Clubb, D. Frail, A. Fruchter, E. Göğüş, J. Greiner, T. Güver, A. Horesh, A. V. Filippenko, S. Klose, J. Mao, A. N. Morgan, A. S. Pozanenko, S. Schmidl, B. Stecklum, M. Tanga, A. A. Volnova, A. E. Volvach, J. G. Wang, J. M. Winters, and Y. X. Xin, *Astrophys. J.* **781**, 37 (2014).
- 68 D. Burlon, G. Ghirlanda, G. Ghisellini, D. Lazzati, L. Nava, M. Nardini, and A. Celotti, *Astrophys. J.* **685**, L19 (2008).
- 69 E. Troja, S. Rosswog, and N. Gehrels, *Astrophys. J.* **723**, 1711 (2010).
- 70 Y.-D. Hu, E.-W. Liang, S.-Q. Xi, F.-K. Peng, R.-J. Lu, L.-Z. Lü, and B. Zhang, *Astrophys. J.* **789**, 145 (2014).
- 71 B. Zhang, Y. Z. Fan, J. Dyks, S. Kobayashi, P. Mészáros, D. N. Burrows, J. A. Nousek, and N. Gehrels, *Astrophys. J.* **642**, 354 (2006).
- 72 Y. Liu, H. Sun, D. Xu, D. S. Svinikin, J. Delaunay, N. R. Tanvir, H. Gao, C. Zhang, Y. Chen, X. F. Wu, B. Zhang, W. Yuan, J. An, G. Bruni, D. D. Frederiks, G. Ghirlanda, J. W. Hu, A. Li, C. K. Li, J. D. Li, D. B. Malesani, L. Piro, G. Raman, R. Ricci, E. Troja, S. D. Vergani, Q. Y. Wu, J. Yang, B. B. Zhang, Z. P. Zhu, A. de Ugarte Postigo, A. G. Demin, D. Dobie, Z. Fan, S. Y. Fu, J. P. U. Fynbo, J. J. Geng, G. Gianfagna, Y. D. Hu, Y. F. Huang, S. Q. Jiang, P. G. Jonker, Y. Julakanti, J. A. Kennea, A. A. Kokomov, E. Kuulkers, W. H. Lei, J. K. Leung, A. J. Levan, D. Y. Li, Y. Li, S. P. Littlefair, X. Liu, A. L. Lysenko, Y. N. Ma, A. Martin-Carrillo, P. O'Brien, T. Parsotan, J. Quirrola-Vasquez, A. V. Ridnaia, S. Ronchini, A. Rossi, D. Mata-Sanchez, B. Schneider, R. F. Shen, A. L. Thakur, A. Tohuvavohu, M. A. P. Torres, A. E. Tsvetkova, M. V. Ulanov, J. J. Wei, D. Xiao, Y. H. I. Yin, M. Bai, V. Burwitz, Z. M. Cai, F. S. Chen, H. L. Chen, T. X. Chen, W. Chen, Y. F. Chen, Y. H. Chen, H. Q. Cheng, C. Z. Cui, W. W. Cui, Y. F. Dai, Z. G. Dai, J. Eder, D. W. Fan, C. Feldman, H. Feng, Z. Feng, P. Friedrich, X. Gao, J. Guan, D. W. Han, J. Han, D. J. Hou, H. B. Hu, T. Hu, M. H. Huang,

- J. Huo, I. Hutchinson, Z. Ji, S. M. Jia, Z. Q. Jia, B. W. Jiang, C. C. Jin, G. Jin, J. J. Jin, A. Keereman, H. Lerman, J. F. Li, L. H. Li, M. S. Li, W. Li, Z. D. Li, T. Y. Lian, E. W. Liang, Z. X. Ling, C. Z. Liu, H. Y. Liu, H. Q. Liu, M. J. Liu, Y. R. Liu, F. J. Lu, H. J. LU, L. D. Luo, F. L. Ma, J. Ma, J. R. Mao, X. Mao, M. McHugh, N. Meidinger, K. Nandra, J. P. Osborne, H. W. Pan, X. Pan, M. E. Ravasio, A. Rau, N. Rea, U. Rehman, J. Sanders, A. Santovincenzo, L. M. Song, J. Su, L. J. Sun, S. L. Sun, X. J. Sun, Y. Y. Tan, Q. J. Tang, Y. H. Tao, J. Z. Tong, H. Wang, J. Wang, L. Wang, W. X. Wang, X. F. Wang, X. Y. Wang, Y. L. Wang, Y. S. Wang, D. M. Wei, R. Willingale, S. L. Xiong, H. T. Xu, J. J. Xu, X. P. Xu, Y. F. Xu, Z. Xu, C. B. Xue, Y. L. Xue, A. L. Yan, F. Yang, H. N. Yang, X. T. Yang, Y. J. Yang, Y. W. Yu, J. Zhang, M. Zhang, S. N. Zhang, W. D. Zhang, W. J. Zhang, Y. H. Zhang, Z. Zhang, Z. Zhang, Z. L. Zhang, D. H. Zhao, H. S. Zhao, X. F. Zhao, Z. J. Zhao, L. X. Zhou, Y. L. Zhou, Y. X. Zhu, Z. C. Zhu, and X. X. Zuo, (2024), arXiv: 2404.16425
- 73 D. K. Galloway and L. Keek, in *Timing Neutron Stars: Pulsations, Oscillations and Explosions, Vol. 461, Astrophysics and Space Science Library Series*, 209, (Springer-Verlag, Berlin, 2021).
- 74 S. J. Prentice, K. Maguire, S. J. Smartt, M. R. Magee, P. Schady, S. Sim, T. W. Chen, P. Clark, C. Colin, M. Fulton, O. McBrien, D. O'Neill, K. W. Smith, C. Ashall, K. C. Chambers, L. Denneau, H. A. Flewelling, A. Heinze, T. W. S. Holoiien, M. E. Huber, C. S. Kochanek, P. A. Mazzali, J. L. Prieto, A. Rest, B. J. Shappee, B. Stalder, K. Z. Stanek, M. D. Stritzinger, T. A. Thompson, and J. L. Tonry, *Astrophys. J.* **865**, L3 (2018).